Fractional solubility of iron in mineral dust aerosols over coastal Namibia: a link to marine biogenic emissions?

Karine Desboeufs, Paola Formenti, Raquel Torres-Sánchez, Kerstin Schepanski, Jean-Pierre Chaboureau, Hendrik Andersen, Jan Cermak, Stefanie Feuerstein, Benoit Laurent, Danitza Klopper, et al.

Atmos. Chem. Phys., 24, 1525–1541, 2024
https://doi.org/10.5194/acp-24-1525-2024

Atmospheric Chemistry and Physics
Open Access
EGU

Fractional solubility of iron in mineral dust aerosols over coastal Namibia: a link to marine biogenic emissions?

Karine Desboeufs[1], Paola Formenti[1], Raquel Torres-Sánchez[2,3], Kerstin Schepanski[4,b], Jean-Pierre Chaboureau[5], Hendrik Andersen[6,7], Jan Cermak[6,7], Stefanie Feuerstein[4], Benoit Laurent[1], Danitza Klopper[8,a], Andreas Namwoonde[9], Mathieu Cazaunau[2], Servanne Chevaillier[2], Anaïs Feron[1,c], Cécile Mirande-Bret[1], Sylvain Triquet[1], and Stuart J. Piketh[8]

[1]LISA, Université Paris Cité and Université Paris Est Créteil, CNRS, 75013 Paris, France
[2]LISA, Université Paris Est Créteil and Université Paris Cité, CNRS, 94010 Créteil, France
[3]CIQSO, Robert H. Grubbs Building, University of Huelva, Campus El Carmen, E21071 Huelva, Spain
[4]Leibniz Institute for Tropospheric Research (TROPOS), Leipzig, Germany
[5]Laboratoire d'Aérologie (LAERO), Université de Toulouse, CNRS, UT3, IRD Toulouse, France
[6]Institute of Meteorology and Climate Research, Karlsruhe Institute of Technology (KIT), Karlsruhe, Germany
[7]Institute of Photogrammetry and Remote Sensing, Karlsruhe Institute of Technology (KIT), Karlsruhe, Germany
[8]North-West University, School for Geo- and Spatial Sciences, Potchefstroom, South Africa
[9]SANUMARC, University of Namibia, Henties Bay, Namibia
[a]now at: Department of Geography and Environmental Studies, University of Limpopo, Sovenga, South Africa
[b]now at: Institute of Meteorology, Freie Universität Berlin, Berlin, Germany
[c]now at: Université Paris-Saclay, INRAE, AgroParisTech, UMR ECOSYS, Palaiseau, France

Correspondence: Paola Formenti (paola.formenti@lisa.ipsl.fr)

Received: 28 July 2023 – Discussion started: 22 August 2023
Revised: 4 December 2023 – Accepted: 5 December 2023 – Published: 31 January 2024

Abstract. This paper presents the first investigation of the solubility of iron in mineral dust aerosols collected at the Henties Bay Aerosol Observatory (HBAO), in Namibia, from April to December 2017. During the study period, 10 intense dust events occurred. Elemental iron reached peak concentrations as high as 1.5 $\mu g\,m^{-3}$, significantly higher than background levels. These events are attributed to wind erosion of natural soils from the surrounding gravel plains of the Namib desert. The composition of the sampled dust is found to be overall similar to that of aerosols from northern Africa but is characterized by persistent and high concentrations of fluorine which are attributed to local fugitive dust.

The fractional solubility of Fe (%SFe) for both the identified dust episodes and background conditions ranged between 1.3 % and 20 % and averaged at 7.9 % (±4.1 %) and 6.8 (±3.3 %), respectively. Even under background conditions, the %SFe was correlated with that of Al and Si. The solubility was lower between June and August and increased from September onwards during the austral spring. The relation to measured concentrations of particulate MSA (methane sulfonic acid), solar irradiance, and wind speed suggests a possible two-way interaction whereby marine biogenic emissions from the coastal Benguela upwelling to the atmosphere would increase the solubility of iron-bearing dust according to the photo-reduction processes. This first investigation points to the western coast of southern Africa as a complex environment with multiple processes and active exchanges between the atmosphere and the Atlantic Ocean, requiring further research.

Published by Copernicus Publications on behalf of the European Geosciences Union.

1 Introduction

Through the processes of atmospheric transport and deposition, mineral dust is known to provide nutrients and metals to the terrestrial and marine ecosystems (Hooper et al., 2019; Ventura et al., 2021). Amongst those, mineral dust provides iron (Jickells et al., 2005), which plays a major role in the primary productivity of the nutrient-limited oceans, modulating the marine carbon cycle (Hooper et al., 2019) as well as that of key continental ecosystems such as the Amazon rainforest (Reichholf, 1986).

To date, much attention has been paid to the soluble Fe in mineral dust emitted from arid and semi-arid areas in the Northern Hemisphere, in particular the Saharan and Chinese deserts (e.g. Baker et al., 2006; Paris et al., 2010; Takahashi et al., 2011; Rodriguez et al., 2021), where emissions are the most intense (Tegen and Schepanski, 2009). Nonetheless, the Southern Hemisphere accounts for approximately 10 % of the global atmospheric dust loading (Kok et al., 2017). Large sources are found in southern Africa, mostly in Namibia (Kalahari and Namib deserts, Etosha Pan, numerous ephemeral riverbeds along the Namibian coastline) and Botswana (Makgadikgadi Pan) (Prospero et al., 2002; Bryant et al., 2007; Mahowald et al., 2003; Ginoux et al., 2012; Vickery and Eckardt, 2013; Von Holdt et al., 2017).

Previous research has shown that the long-range transport of dust emitted from southern African sources can reach the south-eastern Atlantic and Indian oceans (Swap et al., 1996; Jickells et al., 2005; Bhattachan et al., 2012, 2015; Ito and Kok, 2017). In particular, Gili et al. (2022) demonstrated recently that mineral dust from Namibia can also be transported across the Southern Ocean to eastern Antarctica. Furthermore, the research by Dansie et al. (2022) has suggested that mineral dust from Namibia could dominate the atmospheric deposition to the coastal Benguela Upwelling System (BUS), where biomass burning aerosols, a significant source of soluble Fe for the Southern and Indian oceans (Hamilton et al., 2021; Ito et al., 2021; Liu et al., 2022), are limited by atmospheric stratification (Formenti et al., 2019; Redemann et al., 2021). The inputs of Namibian (and Angolan) dust in the upwelled waters could also modulate the migration of skipjack tuna between the Gulf of Guinea and the equatorial Atlantic by contributing to supporting phytoplankton growth and hence upper trophic levels in this area (Rodriguez et al., 2023).

There are, however, very few data available on the concentrations and compositions of soluble Fe in dust aerosols from southern Africa, both near the sources and over the oceans. Previous research in Namibia focused on soils and sediments (Dansie et al., 2017a, b; Kangueehi, 2021). The Atlantic Meridional Transect (AMT) cruise programme conducted recurrent observations between October and March in the South Atlantic Ocean (Baker et al., 2013), while Heimburger et al. (2013) and Gao et al. (2013) reported sparse measurements of deposited aerosols and in rainwater over the southern Indian Ocean.

Within this context, this paper investigates the fractional solubility of Fe (%SFe) in samples of atmospheric aerosol particles smaller than 10 µm in diameter collected in 2017 at the Henties Bay Aerosol Observatory (HBAO) on the Namibian coast. In Sect. 2 we outline the experimental and analytical methodology for elemental and water-soluble analysis of ions and metals, including iron. We also provide the definition of fractional solubility and the method for estimating the total dust mass. We introduce the supporting tools used to evaluate the source regions of the collected mineral dust, their pathways during transport, and the presence of fog, a recurrent feature of coastal Namibia favouring multi-phase ageing processes. Section 3 provides the results of the analysis. We present the iron-soluble concentrations and solubility and explore their links to the load, emission area and transport of mineral dust, and atmospheric processing. Section 4 discusses the observations, suggesting that the %SFe in the Namibian dust is higher when the MSA (methane sulfonic acid), a tracer of marine biogenic emissions, is also detected in these highest concentrations. This points to the photo-oxidation of DMS (dimethyl sulfide) as a process for increasing the Fe solubility and suggests a possible positive feedback loop of the iron fertilization by dust to the ocean. Section 5 summarizes the findings and suggests directions for future research.

2 Methodology

2.1 Study area

The HBAO (22.09° S, 14.26° E; http://www.hbao.cnrs.fr/, last access: 10 October 2022) is located at the Sam Nujoma Marine and Coastal Resources Research Centre (SANUMARC) of the University of Namibia in Henties Bay, Namibia (Fig. 1).

Three kilometres to the south of the university campus hosting the HBAO is the small town of Henties Bay, with no industrial activity and very little traffic and located approximately 170 km north of Walvis Bay, the major harbour in Namibia. Directly east of the HBAO are the Namibian gravel plains, which are one of the dominant features of the Namib desert together with the sand dunes. Approximately 100 m to the north is the Omaruru riverbed, one of the coastal sources of mineral dust identified by Vickery and Eckardt (2013).

Our previous results show that, at the surface level, the atmosphere at the HBAO is a receptor of different air masses dominated by marine aerosols but also the seasonal occurrence of light-absorbing aerosols from biomass burning or pollution in northern wind regimes and mineral dust detected episodically from various wind directions (Formenti et al., 2018; Klopper et al., 2020, hereafter KL20).

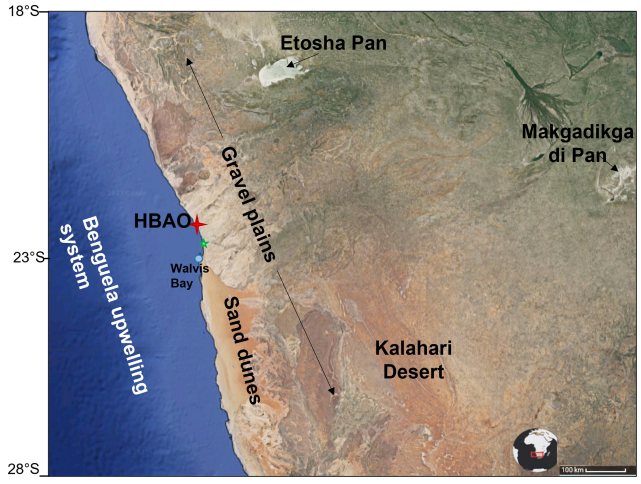

Figure 1. Location of the Henties Bay Aerosol Observatory (HBAO, red star) and the main dust source regions (© Google Maps). The positions of Walvis Bay (blue dot), the major harbour in the area, and the Wlotzkasbaken meteorological station (green star) are also indicated.

2.2 Sample collection and analysis

Aerosol particles smaller than 10 µm in aerodynamic diameter (PM_{10}) were collected by an automated sampler (model Partisol Plus 2025i, Thermo Fisher Scientific, Waltham, MA, USA) on 47 mm Whatman Nuclepore polycarbonate filters (1 µm pore size). The air was drawn through a certified sampling inlet (Rupprecht and Patashnick, Albany, NY, USA) located at approximately 30 m above the ground and operated at a flow rate of 1 $m^3\,h^{-1}$. Samples were collected for 9 h during the daytime (from 09:00 to 18:00 UTC) and nighttime (from 21:00 to 06:00 UTC) for 12 non-consecutive weeks from April to December 2017 (7–14 April, 26 April–3 May, 19–26 May, 7–14 July, 2–9 August, 15–22 August, 18–25 September, 2–9 October, 31 October–7 November, 13–20 November, 28 November–4 December, 12–19 December). In total, 176 samples (+13 blanks, one per week of sampling) were collected.

The elemental analysis of 24 elements from Na to Pb, including some major tracers of mineral dust (Fe, Al, and Si), was performed at the LISA laboratory by wavelength-dispersive X-ray fluorescence (WD-XRF) using a PW-2404 spectrometer (Panalytical, Almelo, Netherlands), as detailed by KL20. The total mass concentration per element x will be referred to as TX.

The measured elemental concentrations are used to calculate the estimated dust mass (EDM) according to Lide (1992) as

$$\begin{aligned}\mathrm{EDM} = 1.12 \times \{&1.658 \times [\mathrm{nss-Mg}] + 1.889 \times [\mathrm{Al}] + 2.139 \\ &\times [\mathrm{Si}] + 1.399 \times [\mathrm{nss-Ca}] + 1.668 \times [\mathrm{Ti}] \\ &+ 1.582 \times [\mathrm{Mn}] + (0.5 \times 1.286 + 0.5 \times 1.429 \\ &+ 0.47 \times 1.204) \times [\mathrm{Fe}]\}, \end{aligned} \quad (1)$$

where, as explained by KL20, nss-Mg and nss-Ca represent the non-sea-salt fractions of Mg and Ca, respectively.

The analysis of the water-soluble fraction was also performed at LISA. Individual filters were placed in 20 mL of ultrapure water (MilliQ® 18.2 MΩ cm) for 30 min. The solution was filtered (Nuclepore polycarbonate filters with 0.2 µm pore size) and then divided into two sub-samples. One-half was analysed by ion chromatography (IC) using a Metrohm IC 850 device equipped with a column MetrosepA supp 7 (250/4.0 mm) for anions and with a Metrosep C4 (250/4.0 mm) for cations. The IC analysis provided the concentrations of the following water-soluble ions: F^-, Cl^-, NO_3^-, SO_4^{2-}, formate, acetate, oxalate, MSA^- (methanesulfonic acid), Na^+, NH_4^+, K^+, Ca^{2+}, and Mg^{2+}. A calibration with certified standard multi-ion solutions of concentrations ranging from 5 to 5000 ppb was performed, and the uncertainty of the analysis was estimated to be 5 % (KL20).

The second half of the solution was acidified to 1 % with ultrapure nitric acid (HNO_3) and analysed by inductively coupled plasma-atomic emission spectroscopy (ICP-AES) using Spectro ARCOS Ametek® ICP-AES and by high-resolution inductively coupled plasma-mass spectrometry (HR-ICP-MS) using a Neptune Plus™ instrument by Thermo Scientific™. The calibration curve was performed using standard multi-element solutions ranging from 2 to 1000 ppb for ICP-AES and from 1 to 1000 ppt for HR-ICP-MS (Desboeufs et al., 2022). These analyses provided the dissolved mass concentrations (DX) of 25 water-soluble metals and metalloids, including Fe, Al, and Si. All sample concentrations were corrected using the filter blanks for each sampling period.

Based on those analyses, the fractional solubility (%SX) representing the percentage solubility value was calculated as

$$\%\mathrm{SX} = 100 \times \mathrm{DX}/\mathrm{TX}, \quad (2)$$

with DX and TX the dissolved and total elemental concentrations, respectively.

Here, a leaching protocol using ultrapure water (UPW) was used to simulate wet deposition of particles, since the wet deposition dominates the total iron supply in the South Atlantic Ocean (Chance et al., 2015). Moreover, the UPW leach enables the chemical reaction between iron with organic or inorganic ligands naturally dissolved from the particulate aerosols into rain droplets. However, it is known that the extraction protocol modulates the dissolution process, and hence the values of %SFe, in particular the estimates using UPW, are higher in comparison to those using seawater but are lower than the acidic, buffered, or reduction agent leach (Perron et al., 2020).

2.3 Ancillary data

Maps of the emission fluxes of mineral dust were calculated using the dust emission model described by Feuerstein and Schepanski (2019) driven by hourly 10 m wind fields on a $0.1° \times 0.1°$ grid from the European Centre for Medium-Range Weather Forecasts (ECMWF). The dust emission parameterization follows Marticorena and Bergametti (1995). Additional information on the soil type was taken from the ISRC soil data set (FAO/IIASA/ISRIC/ISSCAS/JRC, 2012), and information on the aerodynamic roughness length was obtained from POLDER/ADEOS surface products following the works of Marticorena et al. (2004) and Laurent et al. (2005). The MODIS monthly vegetation product (MYD13A3 v6) was used to describe the vegetation cover, while the vegetation type was defined using the BIOME4 database (Kaplan et al., 2003). We additionally differentiated between different dust source types (alluvial beds, dunes, and sand sheets) which allowed us to reflect the source diversity over Namibia and thus the spatial diversity in the soil's susceptibility to wind erosion. This layer was compiled following Feuerstein and Schepanski (2019) using MODIS surface reflectance (MOD09A1 v6). A MODIS-retrieved map on surface water cover was used to eliminate flooded areas as active dust sources.

Back-trajectories of the air masses during the dust events were calculated from the Meso-NH model (version 5.3). The model set-up is similar to the one used for the AErosols, RadiatiOn and CLOuds in southern Africa (AEROCLO-sA) field campaign (Formenti et al., 2019) and related case studies (Flamant et al., 2022; Chaboureau et al., 2022). In short, the model was run on a 5 km grid covering the southern tip of Africa and 67 stretched levels spaced by 60 m close to the surface and by 600 m at high altitude. Meso-NH was run for 24 h for each dust event using initial and boundary conditions provided by the ECMWF operational analysis. Emission, transport, and deposition of dust are described by the scheme of Grini et al. (2006). Back-trajectories were computed online using three passive tracers initialized with the 3D field of their initial conditions. Further details on the dust prognostic scheme, the back-trajectories, and the physical parameterizations are given in Chaboureau et al. (2022).

The presence of fog and low clouds (FLCs) along the Namibian coastline during dust events was analysed using an existing satellite-based fog and low-cloud data set (Andersen et al., 2019). The FLC detection algorithm used to create this data set was developed and validated specifically for this region. The algorithm is based on infrared observations from the Spinning Enhanced Visible and Infrared Imager (SEVIRI) aboard the geostationary Meteosat Second Generation (MSG) satellites, making use of both spectral and textural information. The FLC product is available at the native spatial and temporal resolutions of the SEVIRI sensor (3 km nadir, every 15 min), as described in Andersen and Cermak (2018). The FLC product does not specifically distinguish between fog and low clouds but captures the coastal boundary-layer cloud regime typical of the region and at the HBAO that could interact with mineral dust. It has been shown to be consistent with synoptic-scale atmospheric dynamics (Andersen et al., 2020). The FLC data are used to calculate maps of average fog and low cloud coverage for the time periods of all the dust events given in Table 1.

Observations of the local meteorology, including measurements of air temperature, relative humidity, and fog, at the nearby Wlotzkasbaken meteorological station (22.31° S, 14.45° E; 73 m a.s.l.; see Fig. 1), part of the Southern African Science Service Centre for Climate Change and Adaptive Land Management (SASSCAL) ObservationNet (https://www.sasscal.org/, last access: 14 April 2023), are used.

3 Results

3.1 Description of the dust episodes

The data set discussed in this paper is based on 176 aerosol samples collected at the HBAO, 42 of which were associated with 10 dust episodes. As detailed by KL20, events of mineral dust were identified as peaks in the time series of the mass concentrations of Al and non-sea-salt Ca^{2+} (nss-Ca^{2+}). The dust episodes investigated in this study are a subset of those presented by KL20. We therefore use their naming convention to facilitate the connections between the two papers (Table 1). In the following, we refer to samples collected during the dust episodes as "dust". Samples collected outside the dust events will be indicated as "background".

The dust episodes were long-lasting (generally a few days). The dynamics of the emissive areas, air mass transport, and fog coverage during the episodes (Fig. 2 and Fig. S1 in the Supplement) are driven by the synoptic circulation, which, in southern Africa, is primarily affected by the high-pressure belt under the descending limb of the Hadley cell (Tyson and Preston-Whyte, 2014). The maps of dust emission fluxes and the air mass back-trajectories reflect this seasonality. During the first part of the year (the Dust 04 to 05 episodes), dust emissions originated from the gravel plains and the Etosha Pan north of the HBAO. During this time of the year the transport to the HBAO below 300 m a.s.l. was north- to south-easterly, originating inland from the coast.

From July onwards, the active source areas were identified in the southern gravel plains, Namib sand dunes, and Kalahari desert (this former source only for the Dust 11 to 13 episodes). Air mass transport was southerly and travelled over the sea and along the coastline. It is worth noticing that all the air masses experienced maritime air during their last hours of transport, including the Dust 04 and 05 episodes associated with berg wind conditions, due to the coastal low that develops to the west of the HBAO.

The formation of fog events at Henties Bay is also highly seasonal. The frequency of occurrence of fog events is highest during austral winter at the coast, whereas lifted stratus

Table 1. Dates of dust events identified at the HBAO from May to December 2017 following KL20. The number of samples collected during each episode is indicated in the column called "*N*". The average air temperature, relative humidity, wind speed and direction recorded at the nearby meteorological station in Wlotzkasbaken are reported. The maximum wind speed and corresponding direction are indicated in brackets in the corresponding columns. The average EDM is reported in brackets with the maximum EDM during the event.

Episode identifier	Start and end dates (UTC)	*N*	Air temperature (°C)	RH (%)	Wind speed ($m\,s^{-1}$)	Wind direction (degN)	EDM ($\mu g\,m^{-3}$)
Dust 04	19/05 09:00–20/05 18:00	3	17.7	73.7	2.7 (6.2)	186 (185)	13 (14)
Dust 05	24/05 21:00–26/05 09:00	3	18.1	63.3	2.3 (6.3)	183 (188)	21 (42)
Dust 06	11/07 09:00–13/07 09:00	4	13.2	82.9	1.2 (5.4)	235 (193)	27 (45)
Dust 07	04/08 21:00–06/08 09:00	4	12.5	87.0	1.2 (5.4)	233 (201)	10 (16)
Dust 08	17/08 21:00–19/08 09:00	4	11.9	80.6	1.3 (4.6)	324 (129)	18 (21)
Dust 09	23/09 21:00–24/09 18:00	2	15.6	84.3	3.1 (6.2)	309 (330)	11 (17)
Dust 10	05/10 21:00–08/10 09:00	8	14.0	74.6	2.1 (5.9)	249 (228)	14 (23)
Dust 11	15/11 09:00-18/11 09:00	6	16.7	66.1	3.2 (11.7)	231 (232)	31 (56)
Dust 12	30/11 09:00-01/12 18:00	3	16.7	78.1	1.9 (5.7)	244 (195)	2 (3)
Dust 13	15/12 09:00–19/12 09:00	7	16.9	76.9	2.9 (6.5)	252 (238)	10 (19)

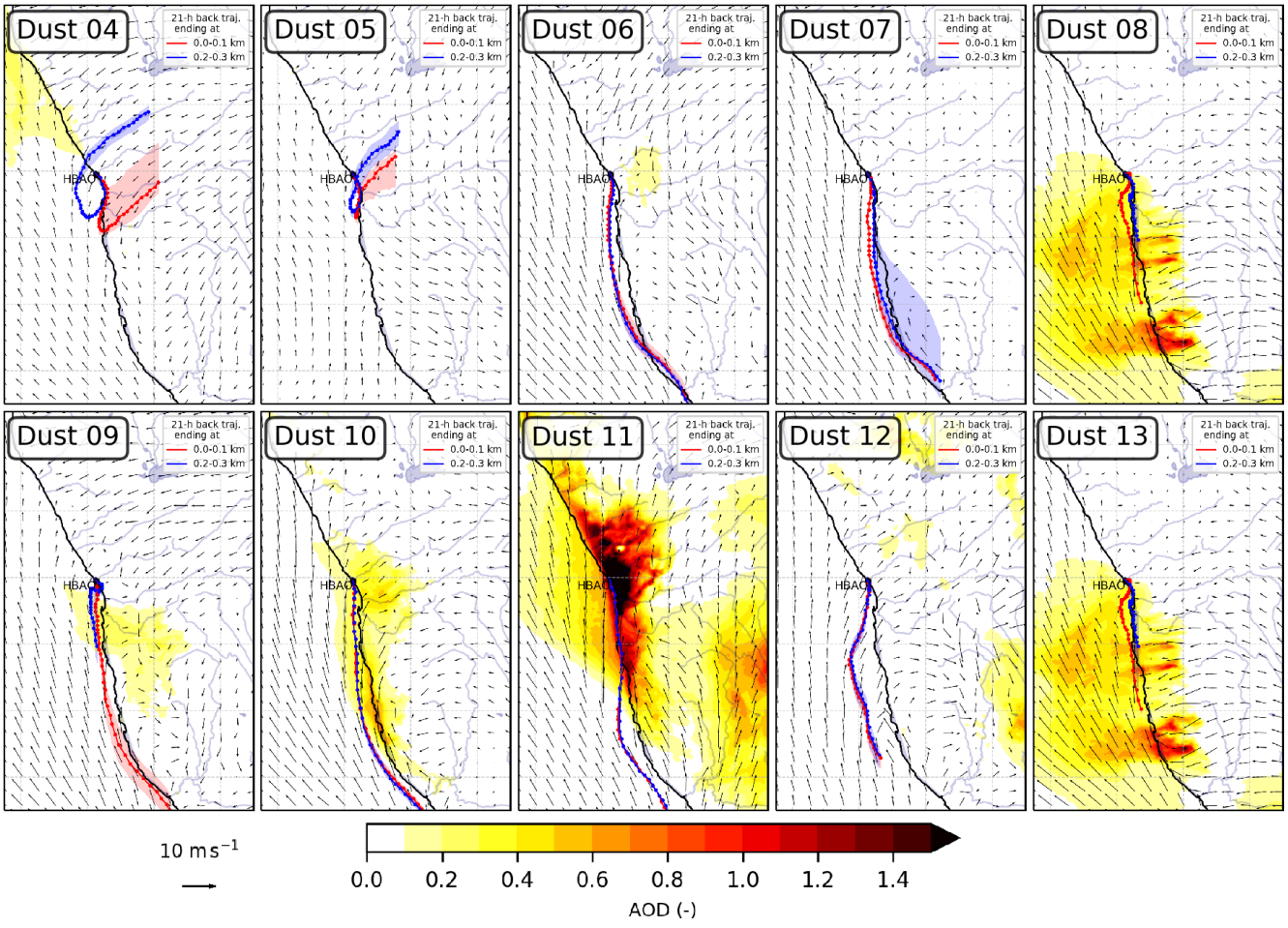

Figure 2. Maps of dust optical depth (shading) and 10 m wind (vector) overlaid by a pathway of 21 h air mass back-trajectories ending in the first 100 m (red line) and between 200 and 300 m (blue line) above the HBAO for dust episodes, as calculated by the Meso-NH model (version 5.3). Dots are plotted every hour, and shadings around these lines are the interquartile ranges for latitudes.

clouds dominate during austral summer, when the overall FLC occurrence peaks. The occurrence of fog over Namibia corresponds to the advection of low-level clouds, which is modulated by both local meteorology along the coastline of Namibia (trade winds) and synoptic-scale radiative processes (Spirig et al., 2019; Andersen et al., 2019, 2020). Henceforth, as shown in Fig. S1, the presence of fog and low clouds correlates with wind directions and aerosol source regions. Overall, three episodes (Dust 04, Dust 05, and Dust 11 in April, May, and November, respectively) occurred under fog-free or low-fog conditions. The remaining episodes were characterized by extensive fog and low cloud coverage throughout the study area. The meteorological observations at the nearby Wlotzkasbaken station (Fig. S2) confirm these findings and show in particular that the relative humidity always exceeded 60 % and 80 % when fog or low clouds were present (Table 1). As a consequence, the aerosol can be considered deliquescent even under the fog-free conditions. The seasonality is also observed in the average downwelling solar irradiance, with the lowest values during July and September associated with austral winter. Finally, it is interesting to note that the fog-free conditions, associated with the predominance of continental air masses, corresponded to the highest EDM, possibly because of the reduced wet removal during transport and the increase in emission fluxes with the decrease in soil moisture (Kok et al., 2014) but possibly also because of the high wind speed prevailing under these conditions, which in principle enhances both dust emissions and transport (Table 1).

3.2 Iron solubility

The total and dissolved concentrations, together with the fractional solubility of Fe, Al, and Si, during the dust episodes are reported in Table 2, where they are compared to background conditions. For iron, the average values over the entire sampling period are also shown.

The total Fe concentrations varied significantly from one episode to another, and so did EDM, which was larger than $10\,\mu g\,m^{-3}$ for all of them (except Dust 12) and as high as $56\,\mu g\,m^{-3}$ during the Dust 11 event (Table 1). By contrast, the total Fe-to-EDM ratio was virtually constant, with averages of 5.8 % (±0.6 %) for the dust events and 5.6 % (±1.1 %) for the entire data set. These values are quite superior to the usual Fe content recommended in upper continental crust models (3.5 % for Taylor and McLennan, 1995; 5.04 ± 0.53 % for Rudnick and Gao, 2004) and estimated in Saharan dust (4.45 % for Guieu et al., 2002; 4.3 % to 6.1 % for Lafon et al., 2006; 4.5 % for Formenti et al., 2008). Keeping in mind that Fe abundance is estimated, this suggests that the Namibian aerosol dust could be enriched in iron in comparison to the upper crust and dust provided by Saharan sources.

The total dissolved concentrations of Fe during the sampling period ranged from 1.5 to $427\,ng\,m^{-3}$, with a median and average of 10.5 and $28\,ng\,m^{-3}$. During the dust episodes, the average mass concentration of dissolved Fe was $80 \pm 84\,ng\,m^{-3}$, almost an order of magnitude higher than for background conditions ($11 \pm 10\,ng\,m^{-3}$). The dissolved concentrations in dust periods are higher than those observed in the South Atlantic Ocean for air masses associated with transport from continental southern Africa (Baker et al., 2013; Chance et al., 2015; Baker and Jickells, 2017), which are of the same order as those observed at the HBAO for background periods. The calculated %SFe ranged from 1.3 % to 19.8 %, with a median and an average of 6.7 % and 7.1 %. The average %SFe during dust events (7.9 ± 4.1 %) was higher than but quite similar to background conditions (6.8 ± 3.3 %). It is interesting to note that the Dust 11 event, the most intense recorded event, presents the highest %SFe (between 10.2 % and 19.8 % with an average at 13.8 %). Apart from this event, the average fractional solubility seems to be independent of the EDM. Excluding this event, the average solubility of Fe for dust events ($6.9\,\% \pm 3.3\,\%$) is equivalent to the one for background samples. The uniformity of %SFe values between background and dust periods contrasted with the observations made in regions where the dust influence is sporadic, and the origin of Fe is associated with various sources (e.g. Shelley et al., 2018). This is consistent with a main dust source of iron in our samples, as indicated in KL20. For both conditions, the observed range of variability is high and consistent with previous observations over the South Atlantic Ocean (2.4 %–20 %, Baker et al., 2013; 1.3 %–22 %, Chance et al., 2015) and the southern Indian Ocean (0.76 %–27 %, Gao et al., 2013) using acetate buffer leach at pH 4.7 (0.4 µm), which can extract 1.4 times more Fe than the UPW protocol (Perron et al., 2020). Moreover, the measured %SFe is significantly higher than that obtained from dissolution experiments, with an identical protocol, of mineral dust aerosol samples collected on filters after laboratory generation from the soils collected in Namibian sources (< 1 %; Paola Formenti, personal communication, 2024).

The temporal variability of %SFe is presented in Fig. 3, where dust and background episodes are shown separately. The temporal variability is similar under dust and background conditions. The highest %SFe occurred during austral spring (October–November) and in particular during the Dust 11 episode from 13 to 20 November 2017, when the average %SFe reached 13.8 %. The %SFe was quite similar along the year between the dust and the background, except between 13 and 20 November, when the iron solubilities during the Dust 11 event were very superior to the one of the background samples and, to a lesser extent, in September (Dust 09) and December (Dust 13).

Figure 4 represents the correlations of Fe with Al and Si for both the total and dissolved concentrations. For both dust and background samples, the total Fe concentration is linearly correlated with the total Al ($R^2 = 0.98$ and 0.96 and slope = 0.75 and 0.71 for dust and background condi-

Table 2. Average and standard deviations of water-soluble (DX) and total elemental (TX) mass concentrations and fractional solubility (%SX) for Fe, Al, and Si at the HBAO measured for the total period and during the dust and background events from April to December 2017. Concentration values are shown ($\mu g\,m^{-3}$), and fractional solubility is shown (%). The number of considered samples is presented in brackets.

	Fe			Al		Si	
	All periods	Dust	Background	Dust	Background	Dust	Background
DX	28 ± 51 ($N = 175$)	80 ± 84 ($N = 42$)	11 ± 10 ($N = 131$)	322 ± 296 ($N = 42$)	56 ± 46 ($N = 131$)	529 ± 616 ($N = 42$)	78 ± 83 ($N = 124$)
TX	364 ± 482 ($N = 176$)	955 ± 633 ($N = 42$)	177 ± 155 ($N = 133$)	1204 ± 870 ($N = 42$)	284 ± 222 ($N = 94$)	4158 ± 3037 ($N = 42$)	776 ± 674 ($N = 133$)
%SX	7.1 ± 3.6 ($N = 175$)	7.9 ± 4.1 ($N = 42$)	6.8 ± 3.3 ($N = 130$)	27 ± 10 ($N = 42$)	26 ± 11 ($N = 90$)	12 ± 7 ($N = 42$)	11 ± 8 ($N = 116$)

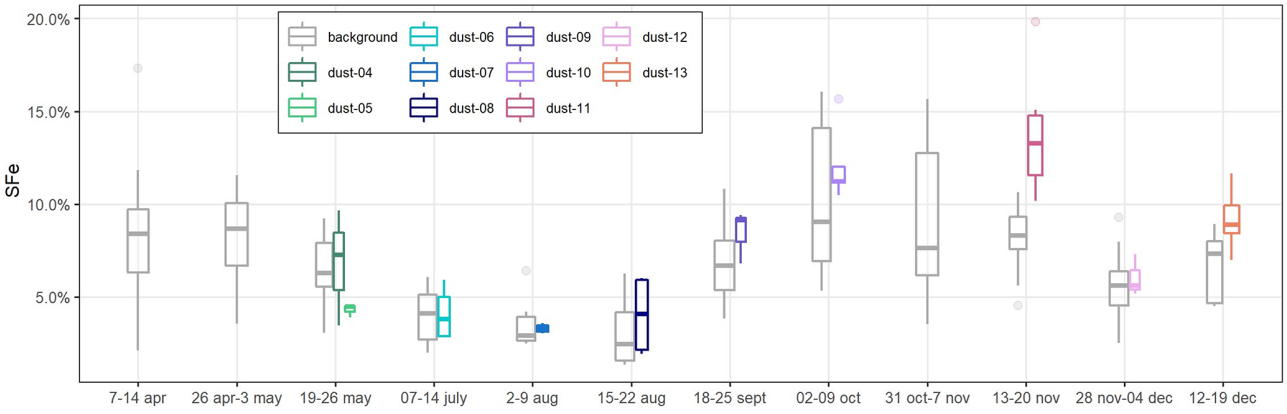

Figure 3. Temporal variability of the %SFe average for dust and background samples during the different periods of sampling. In the boxplots, the box indicates the interquartile range, i.e. the 25th and 75th percentiles, and the line within the box marks the median. The whiskers indicate the quartiles ±1.5 times the interquartile range. Points above and below the whiskers indicate outliers outside the 10th and 90th percentiles.

tions, respectively) and total Si ($R^2 = 0.94$ and 0.97 and slope = 0.21 and 0.23, respectively). The slopes are consistent with typical Fe/Al and Fe/Si ratios found in desert dust from northern Africa (Formenti et al., 2011; Shelley et al., 2015), confirming the main crustal origin of Fe during all the sampling periods. Likewise, the concentrations of dissolved iron (DFe) show a strong linear correlation with both DAl and DSi for both dust and background events ($R^2 = 0.96$ and 0.75 with respect to DAl and $R^2 = 0.98$ and 0.73 with respect to DSi). The slopes for Al and Si are also comparable (0.19 and 0.28 for DAl and 0.10 and 0.13 for DSi, respectively, in dust and in background events). A very strong linear correlation was also observed between DFe and DTi ($R^2 = 0.96$ and 0.84, not shown), another unique marker of mineral dust. Significant correlations of soluble concentrations for several elements associated with mineral dust (Fe, Al, Si, Ti) have been previously obtained in remote aerosols over oceanic areas (Baker et al., 2016). Additionally, DFe during dust events correlate very closely with F^- ($R^2 = 0.94$, not shown), which has been indicated by KL20 as being emitted into the atmosphere by the wind erosion as well as the labouring of the Namibian soil that is rich in fluoride mineral deposits.

4 Discussion

Several studies have shown that variations in aerosol Fe solubility could result from the source and composition of the aerosols. As a matter of fact, the Fe solubility has been linked to the iron mineralogy (Journet et al., 2008) and has been shown to be lower for African crustal sources than in continental and anthropogenic sources (Desboeufs et al., 2005; Sholkovitz et al., 2009; Shelley et al., 2018). The iron fractional solubility in mineral dust is also affected by source mixing (Paris et al., 2010; Desboeufs et al., 2005), by (photo-)chemical processing with acids or organic ligands during atmospheric transport (Paris et al., 2011; Paris and Desboeufs, 2013; Wozniak et al., 2013; Swan and Ivey, 2021) and by the increase in the surface area to volume ratio due to size changes during transport (Baker and Jickells, 2006; Marcotte et al., 2020).

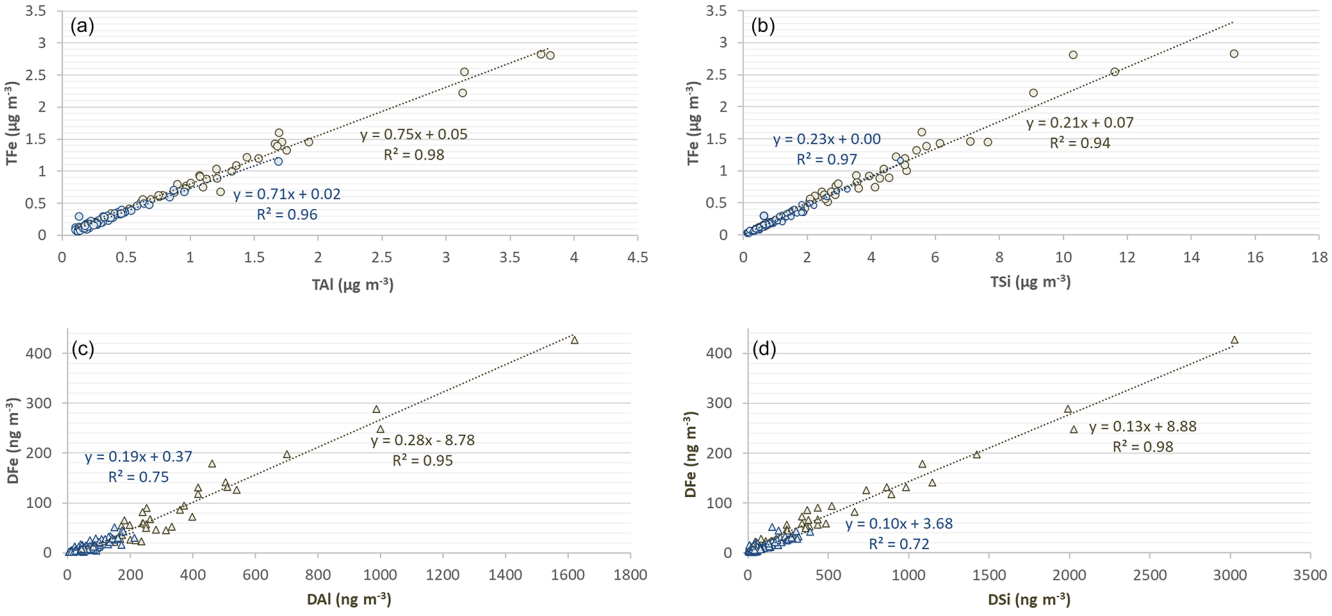

Figure 4. Scatterplot of TFe with respect to TAl and TSi **(a, b)** and DFe with respect to DAl and DSi **(c, d)** for dust (sand dots and triangles) and background events (blue dots and triangles). The Pearson coefficients are shown for both.

In the following sections, we discuss these possible factors to explain the seasonality and extended range of variability of the %SFe in the HBAO samples. The possible increase in the surface area to volume ratio during transport (Baker and Jickells, 2006; Marcotte et al., 2020) will not be discussed because of a lack of appropriate observations of the size distribution. Because of the similar transport time suggested by back-trajectories (Fig. 2), it is likely that the particle size distribution would be similar from one event to another.

4.1 Influence of dust composition

Close to the dust source, iron solubility could be mainly conditioned by the mineralogical composition of dust (Journet et al., 2008; Formenti et al., 2014). Considering that soluble Fe-bearing aerosols were issued from mineral dust for all the samples, the seasonality of dust emission sources (see Sect. 3.1) could be a factor explaining the seasonality of %SFe (and other elements associated with mineral dust). Figure 5 shows the scatterplot of the elemental mass ratio of $\mathrm{Fe/nss-Ca^{2+}}$ and Si/Al previously used for northern African dust to distinguish aerosol dust from source areas enriched in clays or iron oxides and soils rich in quartz or carbonates (Formenti et al., 2014). Specific to Namibia, because of the strong link between nss-$\mathrm{Ca^{2+}}$ and fluorine, the $\mathrm{Fe/nss-Ca^{2+}}$ ratio may also distinguish dust influenced by fluorspar mining.

Figure 5 indicates that the range of variability of both $\mathrm{Fe/nss-Ca^{2+}}$ and Si/Al ratios is small when considering dust events only. The elemental ratios of samples collected during the background periods are rather similar to dust events during the same sampling period, except for Si/Al for the period between 19 and 26 May and for $\mathrm{Fe/nss-Ca^{2+}}$ for the samples of 18–25 September, when significant differences not really explicable and not inducing a significant difference in the %SFe values are observed (Fig. S3).

The values for ambient dust measured at the HBAO are consistent with those of previous field observations in Namibia (Annegarn et al., 1983; Eltayeb et al., 1993) but also with values reported by Caponi et al. (2017) for laboratory-aerosolized dust from two soils collected on the Namibian gravel plains. This is in agreement of the indications of the emission maps (Fig. 2) showing significant emissions on the gravel plains. The absence of seasonal cycles in the elemental composition illustrated in Fig. S3 suggests that the seasonal change from northern to southern sources does not induce a change in the composition of the aerosol dust sampled at the HBAO, which is consistent with the fact that the northern and southern gravel plains of Namibia have similar mineralogy (Heine and Vökel, 2010). This suggests that the mineralogical composition of mineral dust should not be a discriminating factor explaining the seasonality of the iron solubility observed at the HBAO.

4.2 Evidence of processing by marine biogenic emissions

The atmospheric (in-cloud) processing associated with secondary aerosol production may increase the fractional solubility of Fe during transport (Takahashi et al., 2011; Rodríguez et al., 2021). This has also been shown for Al and Ti (Baker et al., 2020). The chemical processing could include

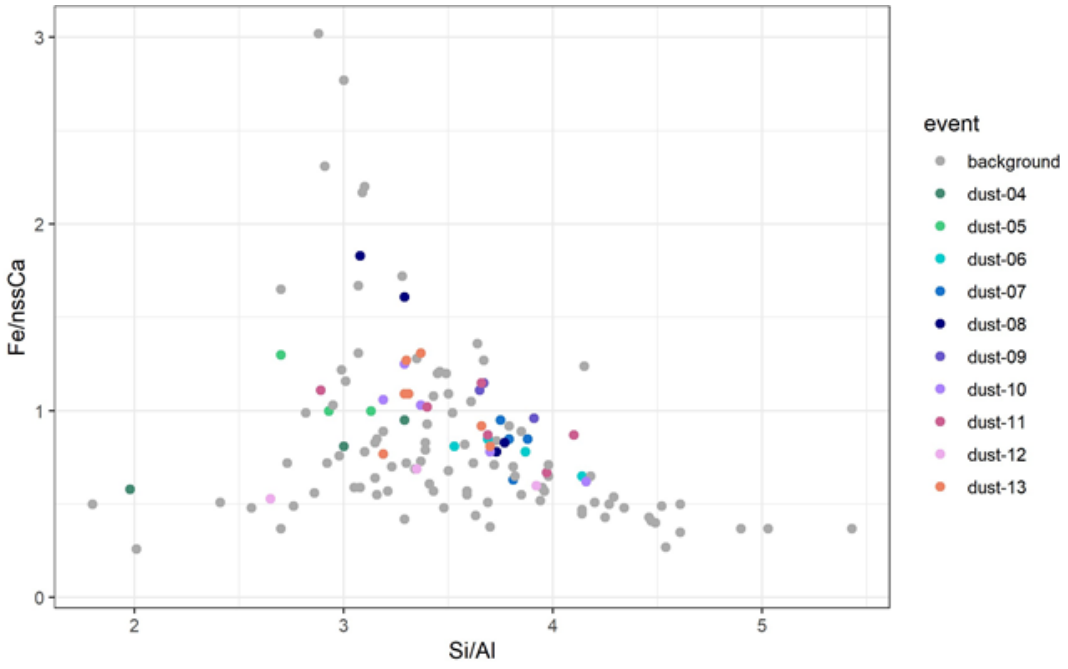

Figure 5. Scatterplot of $Fe/nss - Ca^{2+}$ and Si/Al mass ratios for the samples collected at the HBAO in the period May–December 2017. Values obtained for samples collected during the dust events are represented as coloured dots. Values for samples collected outside those events (background) are represented as grey dots.

both acidic and ligand-promoted dissolution (Desboeufs et al., 2001; Longo et al., 2016; Tao et al., 2019). Oxalic acid has previously been used as a proxy for organic ligand-mediated iron dissolution processes because it is the most abundant species in the atmosphere and is the most effective ligand in promoting iron dissolution (Baker et al., 2020; Hamilton et al., 2021). However, several secondary compounds, such as carboxylate ligands and marine secondary products derived from DMS oxidation, have been identified as playing a role in increasing the soluble fraction of iron from mineral aerosols (Johansen and Key, 2006; Paris et al., 2011; Paris and Desboeufs, 2013; Wozniak et al., 2013, 2015). The increase in ligand-promoted dissolution is attributed to photo-chemical reduction of Fe(III) in Fe (II) (Siefert et al., 1994; Johansen and Key, 2006).

To investigate these aspects, the mass concentrations of the ionic compounds (oxalate, formate, MSA, NO_3^-, NH_4^+, and nss-SO_4^{2-}) implied in the secondary aerosol production, measured at the HBAO during the dust and background periods, are reported in Table 3.

Oxalate was the most abundant organic compound, followed by MSA, a secondary product of DMS oxidation and a unique particulate tracer of the primary marine biogenic activity (Andreae et al., 1995). On average, organic compounds were equally concentrated in dust and background events. Amongst inorganic species, nss-SO_4^{2-} was the most concentrated compound, with higher values during the dust events than during the background period.

Table 3. Average and standard deviations of mass concentrations of water-soluble ions measured at the HBAO during dust and background events from May to December 2017. Concentrations are expressed in nanograms per cubic metre. The number of samples pertaining to each occurrence is indicated in brackets.

	Dust	Background
nss-SO_4^{2-}	1795 ± 762 ($N = 42$)	1366 ± 505 ($N = 132$)
Oxalate	155 ± 53 ($N = 42$)	127 ± 35 ($N = 132$)
Formate	18 ± 6 ($N = 40$)	16 ± 9 ($N = 105$)
MSA	64 ± 37 ($N = 36$)	56 ± 36 ($N = 114$)
NO_3^-	205 ± 79 ($N = 42$)	200 ± 138 ($N = 132$)
NH_4^+	192 ± 71 ($N = 42$)	207 ± 98 ($N = 132$)

The detailed time series of secondary compounds are shown in Fig. 6, where they are compared to that of the %SFe. There is no clear seasonal cycle for any of the ionic compounds, with the exception of MSA, which shows a similar time variability to %SFe. MSA concentrations were lowest between May and August (average 38.0 ± 28.0 ng m^{-3}), while higher concentrations were measured from September to December (72.7 ± 38.1 ng m^{-3}). These differences are also observed for the dust cases only. The average MSA concentration was 40.6 ± 23.4 ng m^{-3} for the Dust 04 to Dust 08 episodes. It increased to 77.7 ± 35.3 ng m^{-3}, almost a factor of 2, between the Dust 09 and Dust 13 episodes. The mass concentrations and the seasonal cycle of MSA are re-

lated to the proximity of the strong coastal upwelling by the Benguela Current (Formenti et al., 2019; KL20). The maximum concentration of MSA (106.2 ng m^{-3}) was measured during the Dust 11 episode, which is also the time of the highest SFe% observation. This episode was also characterized by the highest oxalate, nss-SO_4^{2-}, and NO_3^- concentrations. However, no clear correlation between the %SFe and the secondary compound concentrations can be found in our data (Fig. S4). In order to statistically explore the potential links between %SFe and various parameters, Fig. 7 shows the correspondence plot between the total Fe, Al, and Si and their respective fractional solubility, the measured secondary compounds, and the meteorological conditions during sampling obtained from principal component analysis (PCA) for all the samples. The variables correlated in time are grouped together (the closer they are in the circle, the stronger the correlation), whereas the variables which are anti-correlated are situated on the opposite side of the plot origin.

The PCA plot (Fig. 7) emphasizes three groups of dependent parameters: (1) a high correlation between total Fe, Al, and Si concentrations and dust loading (EDM), as previously identified in Table 1 and Fig. 3; (2) a relation between oxalate and nss-SO_4^{2-} concentrations, suggesting a common chemical process of formation; and (3) the dependence between %SFe (%SAl and %SSi), the MSA concentrations, the solar irradiance, and, to a lesser extent, the wind speed. While it is expected that the emission of mineral dust will occur when the wind speed is high, the correlation of %SFe with wind speed is rather surprising since the %SFe is independent of the dust load (Figs. 2 and 7). Figure S4 presents the plots between %SFe, MSA concentrations, solar irradiance, and wind speed for background and dust events. The correlation between the wind speed and the MSA concentrations (Fig. S4) is consistent with Andreae et al. (1995), who demonstrated how, in this area due to persistent phytoplankton bloom, the atmospheric concentrations of DMS, the gaseous precursors of MSA, depend on the sea-to-air flux, which in turn is determined by the concentrations in the ocean water and the surface wind speed.

As previously mentioned, Johansen and Key (2006) showed an increase in dissolution of ferrihydrite, a proxy of iron(oxy)hydroxide found in desert mineral dust, by photolysis of the Fe(III)–MSIA (methane sulfinic acid) complex, producing MSA and soluble Fe. Zhuang et al. (1992) proposed an increase in iron dissolution by the acidification of aerosol particles associated with DMS oxidation. Here, the link between the %SFe, solar irradiance, and MSA is in agreement with the photo-reduction dissolution of Fe by MSA condensation on Fe-bearing dust. Thus, we attribute the %SFe seasonality observed at the HBAO to both solar irradiance and MSA temporal evolution via this process. It is interesting to note that, due to the high correlation between %SFe, %SAl, and %SSi, the photo-chemical processes could also impact the solubility of all element-bearing dust.

4.3 Link to other sources of iron and oxalate

Formenti et al. (2018) showed that, in the austral winter, when the synoptic circulation is dominantly anti-cyclonic, air masses laden with light-absorbing aerosols either from ship pollution or biomass burning can be transported to the HBAO (Formenti et al., 2018). However, the lowest Fe solubility (< 5 %) was measured in July and August 2017, and no correlation between the %SFe and the percent mass fraction of iron from sources other than dust can be found in our data (not shown).

The mass apportionment of iron reported by KL20 indicates that, during the dust events and the background periods, respectively, 7 % and 29 % of the mass of total elemental Fe was not associated with mineral dust but rather with a factor indicated as an "ammonium-neutralized component" mostly characterized by secondary species and non-sea-salt potassium (nss-K^+). The PMF (positive matrix factorization) analysis indicated that the ammonium-neutralized component was associated with photo-oxidation of marine biogenic emissions but also episodically with biomass burning. This component includes oxalate, the most concentrated organic species at the HBAO and the strongest of the organic ligands promoting the photo-reduction of iron in mineral dust, hence the increase in its fractional solubility (Paris and Desboeufs, 2013). Surprisingly, except for individual cases (Dust 13), our analysis does not show this strong link (Fig. 7), and indeed, in contrast to the SFe%, the oxalate concentrations measured at the HBAO were practically constant with time (on average 0.14 ± 0.04 µg m^{-3}). The possible pathways of oxalate formation in this complex atmosphere are numerous through the year, from natural and anthropogenic sources (marine, heavy-oil combustion, biomass burning) to in-cloud and photo-oxidative processes (Baboukas et al., 2000; Myriokefalitakis et al., 2011).

5 Concluding remarks

For the first time, the fractional solubility of Fe in airborne atmospheric aerosols smaller than 10 µm in diameter is investigated along the western coast of Namibia in southern Africa, a critical region for the global climate.

Ten intense episodes of transport of mineral dust from aeolian erosion were identified from the analysis of aerosol samples collected between May and December 2017 at the Henties Bay Aerosol Observatory (HBAO). Based on modelling and measurements, source regions were identified in both the northern and southern gravel plains. Our data do not provide any evidence of the possible contribution of dust from coastal riverbeds, which are considered to be frequent sources of atmospheric dust and soluble iron in the region (Vickery et al., 2013; Von Holdt et al., 2017; Dansie et al., 2017a, b). The total iron represents, on average, 5.8 % (±0.6 %) of the total dust mass, and the average water-soluble Fe fractional solubility is 6.9 % (±3.3 %). These values should be useful to

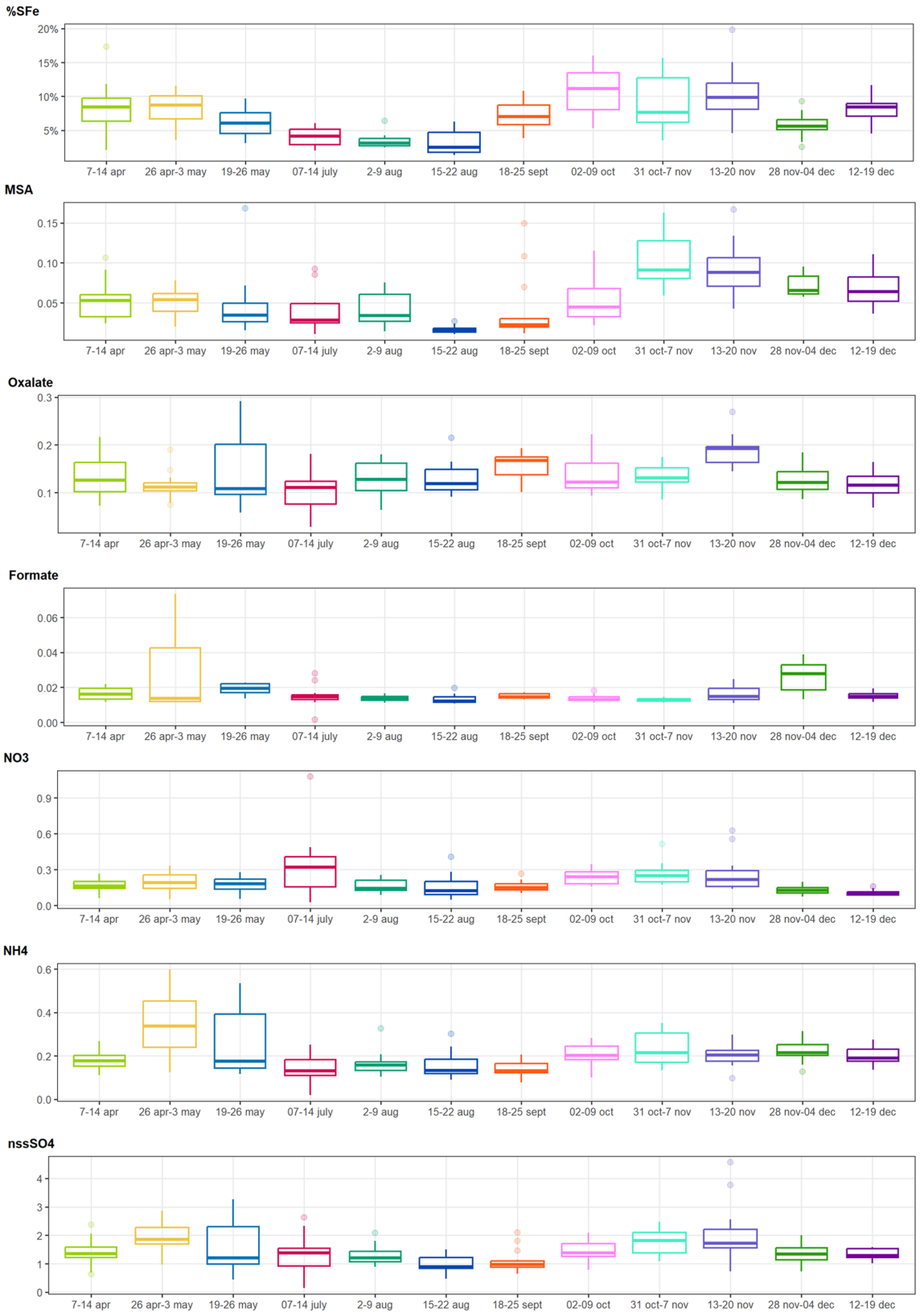

Figure 6. Boxplots of the averages of %SFe and secondary organic and inorganic compound mass concentrations (µg m^{-3}) for the sampling periods including all the samples (dust + background). Boxes and whiskers as in Fig. 3.

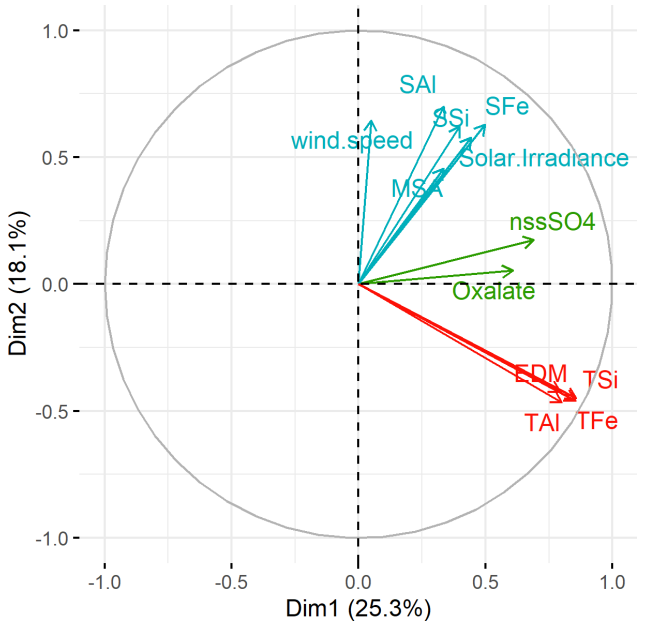

Figure 7. PCA performed from the database including %SX, TX, EDM, secondary ion concentrations, and meteorological parameters. The colour of variables by groups is defined by a clustering algorithm, tending to find clusters of a comparable spatial extent. Each colour corresponds to a cluster of parameters which evolve in the same way. Formate, nitrate, ammonium, acetate, humidity, and wind speed are not visible in the plot, showing that they are not significantly correlated with the other parameters (i.e. their squared cosine < 0.4).

atmospheric models estimating the dust-borne input of soluble Fe from the gravel plains in Namibia to the surrounding oceans.

The seasonal increase in %SFe is associated with that of the concentrations of MSA and is correlated with meteorological parameters such as the wind speed and the surface solar irradiance. Our observations support the role of photo-chemical processes in the dissolution of Fe in our samples and suggest that the oxidation of the marine biogenic emissions from the northern Benguela upwelling, favoured under high wind speed conditions, could play a significant role in increasing the solubility of elemental iron in mineral dust aerosols over coastal Namibia. This is in agreement with the mechanism described by Zhuang et al. (1992), who proposed an increase in iron dissolution by the acidification of aerosol particles associated with DMS oxidation, and Johansen and Key (2006), who showed an increase in the dissolution of ferrihydrite, a proxy of iron(oxy)hydroxide found in desert mineral dust, by photolysis of the Fe(III)–MSIA (methane sulfinic acid) complex, producing MSA and soluble Fe. It is interesting to note that, due to the high correlation between %SFe, %SAl, and %SSi (and %STi), the same photo-chemical processes could also impact the solubility of all element-bearing dust. The possible mechanism suggested by this paper could be responsible for initiating a feedback loop whereby the input of dust of increased trace and major element solubility would result in stronger marine biogenic emissions into the atmosphere. This possible mechanism could increase the iron solubility in mineral dust, maybe also initiating a feedback loop whereby the input of dust of increased solubility would result in stronger marine biogenic emissions into the atmosphere, including volatile organic compounds, in particular butene, massively emitted by organisms in the coastal marine foam (Giorio et al., 2022). This complex and dynamic environment with the interplay between the input of atmospheric iron from transported dust and the marine biogenic emissions from the Benguela oceanic upwelling system should be further addressed by future research.

Code and data availability. Atmospheric concentrations of total and dissolved elements and water-soluble ions measured over coastal Namibia in 2017 are available in Easy Data (Formenti et al., 2023, https://doi.org/10.57932/2ac79cd1-282a-4004-87d5-38f0ebcaf40c). All PCA analyses were performed using the FactoMineR R package (https://doi.org/10.18637/jss.v025.i01, Le et al., 2008). Meteorological data from the Wlotzkasbaken station (22.31° S, 14.45° E; 73 m a.s.l.) are part of the Southern African Science Service Centre for Climate Change and Adaptive Land Management (SASSCAL) ObservationNet (https://www.sasscalweathernet.org/weatherstat_hourly_we.php?, last access: 18 January 2024).

Supplement. The supplement related to this article is available online at: https://doi.org/10.5194/acp-24-1525-2024-supplement.

Author contributions. PF, DK, SJP, AN, MC, AF, and SC prepared and performed the filter sampling. RTS, KD, PF, SC, ST, and CMB performed the XRF, IC, and ICP analyses of the collected samples. BL performed the field implementation. KS and SF performed the model calculations of dust emission fluxes. JPC performed the model calculations of air mass back-trajectories. HA and JC provided the satellite retrieval of fog and low clouds. PF, KD, RTS, and SJP analysed and interpreted the data set. PF and KD wrote the paper with contributions from RTS and SJP as well as the remaining authors. PF and SJP provided funding. PF coordinated the research activity and supervised its planning and execution.

Competing interests. At least one of the (co-)authors is a guest member of the editorial board of *Atmospheric Chemistry and Physics* for the special issue "New observations and related modelling studies of the aerosol–cloud–climate system in the Southeast Atlantic and southern Africa regions (ACP/AMT inter-journal SI)". The peer-review process was guided by an independent editor, and the authors also have no other competing interests to declare.

Special issue statement. This article is part of the special issue "New observations and related modelling studies of the aerosol–cloud–climate system in the Southeast Atlantic and southern Africa regions (ACP/AMT inter-journal SI)". It is not associated with a conference.

Acknowledgements. Danitza Klopper acknowledges the financial support of the Climatology Research Group of North-West University and a travel scholarship of the French Embassy in South Africa (internship at LISA in summer 2018). Raquel Torres-Sánchez acknowledges the Postdoctoral Fellowship Margarita Alsolas (University of Huelva) funded by the Ministry of Universities of Spain (NextGenerationEU). The SASSCAL ObservationNet (https://www.sasscal.org/, last access: 14 April 2023) is acknowledged for open-access data provision. The authors would also like to acknowledge the support by the IPGP platform PARI for HR-ICP-MS analysis. Fadi Lahmidi and Zirui Zeng (LISA) are acknowledged for support in the ion chromatography analysis.

Financial support. This work received funding from the French Centre National de la Recherche Scientifique (CNRS) and the South African National Research Foundation (NRF) through the Groupement de Recherche Internationale Atmospheric Research in southern Africa and the Indian Ocean (GDRI-ARSAIO), the Project International de Coopération Scientifique (PICS) "Long-term observations of aerosol properties in Southern Africa" (contract no. 260888), and the Partenariats Hubert Curien (PHC) PROTEA of the French Minister of Foreign Affairs and International Development (contract nos. 33913SF and 38255ZE).

Review statement. This paper was edited by Luis A. Ladino and reviewed by Rachel Shelley and Sergio Rodríguez.

References

Andersen, H. and Cermak, J.: First fully diurnal fog and low cloud satellite detection reveals life cycle in the Namib, Atmos. Meas. Tech., 11, 5461–5470, https://doi.org/10.5194/amt-11-5461-2018, 2018.

Andersen, H., Cermak, J., Solodovnik, I., Lelli, L., and Vogt, R.: Spatiotemporal dynamics of fog and low clouds in the Namib unveiled with ground- and space-based observations, Atmos. Chem. Phys., 19, 4383–4392, https://doi.org/10.5194/acp-19-4383-2019, 2019.

Andersen, H., Cermak, J., Fuchs, J., Knippertz, P., Gaetani, M., Quinting, J., Sippel, S., and Vogt, R.: Synoptic-scale controls of fog and low-cloud variability in the Namib Desert, Atmos. Chem. Phys., 20, 3415–3438, https://doi.org/10.5194/acp-20-3415-2020, 2020.

Andreae, M. O., Elbert, W., and de Mora, S. J.: Biogenic sulfur emissions and aerosols over the tropical South Atlantic: 3. Atmospheric dimethylsulfide, aerosols and cloud condensation nuclei, J. Geophys. Res., 100, 11335–11356, https://doi.org/10.1029/94JD02828, 1995.

Annegarn, H. J., van Grieken, R. E., Bibby, D. M., and von Blottnitz, F.: Background Aerosol Composition in the Namib Desert, South West Africa (Namibia), Atmos. Environ., 17, 2045–2053, https://doi.org/10.1016/0004-6981(83)90361-X, 1983.

Baboukas, E. D., Kanakidou, M., and Mihalopoulos, N.: Carboxylic acids in gas and particulate phase above the Atlantic Ocean, J. Geophys. Res., 105, 14459–14471, https://doi.org/10.1029/1999JD900977, 2000.

Baker, A. R. and Jickells, T. D.: Mineral particle size as a control on aerosol iron solubility, Geophys. Res. Lett., 33, L17608, https://doi.org/10.1029/2006GL026557, 2006.

Baker, A. R. and Jickells, T. D.: Atmospheric deposition of soluble trace elements along the Atlantic Meridional Transect (AMT), in The Atlantic Meridional Transect programme (1995–2016), Prog. Oceanogr., 158, 41–51, https://doi.org/10.1016/j.pocean.2016.10.002, 2017.

Baker, A. R., Jickells, T. D., Witt, M., and Linge, K. L.: Trends in the solubility of iron, aluminium, manganese and phosphorus in aerosol collected over the Atlantic Ocean, Mar. Chem., 98, 43–58, https://doi.org/10.1016/j.marchem.2005.06.004, 2006.

Baker, A. R., Adams, C., Bell, T. G., Jickells, T. D., and Ganzeveld, L.: Estimation of atmospheric nutrient inputs to the Atlantic Ocean from 50° N to 50° S based on large-scale field sampling: iron and other dust-associated elements, Global Biogeochem. Cy., 27, 755–767, https://doi.org/10.1002/gbc.20062, 2013.

Baker, A. R., Thomas, M., Bange, H. W., and Plasencia Sánchez, E.: Soluble trace metals in aerosols over the tropical southeast Pacific offshore of Peru, Biogeosciences, 13, 817–825, https://doi.org/10.5194/bg-13-817-2016, 2016.

Baker, A. R., Li, M., and Chance, R.: Trace metal fractional solubility in size-segregated aerosols from the tropical eastern Atlantic Ocean, Global Biogeochem. Cy., 34, e2019GB006510, https://doi.org/10.1029/2019GB006510, 2020.

Bhattachan, A., D'Odorico, P., Baddock, M. C., Zobeck, T. M., Okin, G. S., and Cassar, N.: The Southern Kalahari: a potential new dust source in the Southern hemisphere?, Environ. Res. Lett., 7, 024001, https://doi.org/10.1088/1748-9326/7/2/024001, 2012.

Bhattachan, A., D'Odorico, P., and Okin, G. S.: Biogeochemistry of dust sources in Southern Africa, J. Arid Environ., 117, 18–27, https://doi.org/10.1016/j.jaridenv.2015.02.013, 2015.

Bryant, R. G., Bigg, G. R., Mahowald, N. M., Eckardt, F. D., and Ross, S. G.: Dust emission response to climate in southern Africa, J. Geophys. Res., 112, D09207, https://doi.org/10.1029/2005JD007025, 2007.

Caponi, L., Formenti, P., Massabó, D., Di Biagio, C., Cazaunau, M., Pangui, E., Chevaillier, S., Landrot, G., Andreae, M. O., Kandler, K., Piketh, S., Saeed, T., Seibert, D., Williams, E., Balkanski, Y., Prati, P., and Doussin, J.-F.: Spectral- and size-resolved mass absorption efficiency of mineral dust aerosols in the shortwave spectrum: a simulation chamber study, Atmos. Chem. Phys., 17, 7175–7191, https://doi.org/10.5194/acp-17-7175-2017, 2017

Chaboureau, J.-P., Labbouz, L., Flamant, C., and Hodzic, A.: Acceleration of the southern African easterly jet driven by the radiative effect of biomass burning aerosols and its impact on transport during AEROCLO-sA, Atmos. Chem. Phys., 22, 8639–8658, https://doi.org/10.5194/acp-22-8639-2022, 2022.

Chance, R., Jickells, T. D., and Baker, A. R.: Atmospheric trace metal concentrations, solubility and deposition fluxes in remote marine air over the south-east Atlantic, Mar. Chem., 177, 45–56, https://doi.org/10.1016/j.marchem.2015.06.028, 2015.

Dansie, A. P., Wiggs, G. F. S., Thomas, D. S. G., and Washington, R.: Measurements of windblown dust characteristics and ocean fertilisation potential: The ephemeral river valleys of Namibia, Aeolian Res., 29, 30–41, https://doi.org/10.1016/j.aeolia.2017.08.002, 2017a.

Dansie, A. P., Wiggs, G. F. S., and Thomas, D. S. G.: Iron and nutrient content of wind-erodible sediment in the ephemeral river valleys of Namibia, Geomorphology, 290, 335–346, https://doi.org/10.1016/j.geomorph.2017.03.016, 2017b.

Dansie, A. P., Thomas, D. S. G., Wiggs, G. F. S., Baddock, M. C., and Ashpole, I.: Plumes and blooms – Locally-sourced Fe-rich aeolian mineral dust drives phytoplankton growth off southwest Africa, Sci Total Environ., 829, 154562, https://doi.org/10.1016/j.scitotenv.2022.154562, 2022.

Desboeufs, K. V., Losno, R., and Colin, J. L.: Factors influencing aerosol solubility during cloud processes, Atmos. Environ., 35, 3529–3537, https://doi.org/10.1016/S1352-2310(00)00472-6, 2001.

Desboeufs, K. V., Sofikitis, A., Losno, R., Colin, J. L., and Ausset, P.: Dissolution and solubility of trace metals from natural and anthropogenic aerosol particulate matter, Chemosphere, 58, 195–203, 2005.

Desboeufs, K., Fu, F., Bressac, M., Tovar-Sánchez, A., Triquet, S., Doussin, J.-F., Giorio, C., Chazette, P., Disnaquet, J., Feron, A., Formenti, P., Maisonneuve, F., Rodríguez-Romero, A., Zapf, P., Dulac, F., and Guieu, C.: Wet deposition in the remote western and central Mediterranean as a source of trace metals to surface seawater, Atmos. Chem. Phys., 22, 2309–2332, https://doi.org/10.5194/acp-22-2309-2022, 2022.

Eltayeb, M. A., Van Grieken, R. E., Maenhaut, W., and Annegarn, H. J.: Aerosol-Soil Fractionation for Namib Desert Samples, Atmos. Environ., 27, 669–678, https://doi.org/10.1016/0960-1686(93)90185-2, 1993.

FAO/IIASA/ISRIC/ISSCAS/JRC: Harmonized World Soil Database (version 1.2), FAO, Rome, Italy and IIASA, Luxenburg, Austria, http://webarchive.iiasa.ac.at/Research/LUC/External-World-soil-database/HTML/ (last access: 18 January 2024), 2012.

Feuerstein, S. and Schepanski, K.: Identification of Dust Sources in a Saharan Dust Hot-Spot and Their Implementation in a Dust-Emission Model, Remote Sens., 11, 4, https://doi.org/10.3390/rs11010004, 2019.

Flamant, C., Gaetani, M., Chaboureau, J.-P., Chazette, P., Cuesta, J., Piketh, S. J., and Formenti, P.: Smoke in the river: an Aerosols, Radiation and Clouds in southern Africa (AEROCLO-sA) case study, Atmos. Chem. Phys., 22, 5701–5724, https://doi.org/10.5194/acp-22-5701-2022, 2022.

Formenti, P., Rajot, J.-L., Desboeufs, K., Caquineau, S., Chevaillier, S., Nava, S., Gaudichet, A., Journet, E., Triquet, S., Alfaro, S., Chiari, M., Haywood, J., Coe, H., and Highwood, E.: Regional variability of the composition of mineral dust from western Africa: Results from the AMMA SOP0/DABEX and DODO field campaigns, J. Geophys. Res., 113, D00C13, https://doi.org/10.1029/2008JD009903, 2008

Formenti, P., Schütz, L., Balkanski, Y., Desboeufs, K., Ebert, M., Kandler, K., Petzold, A., Scheuvens, D., Weinbruch, S., and Zhang, D.: Recent progress in understanding physical and chemical properties of African and Asian mineral dust, Atmos. Chem. Phys., 11, 8231–8256, https://doi.org/10.5194/acp-11-8231-2011, 2011.

Formenti, P., Caquineau, S., Desboeufs, K., Klaver, A., Chevaillier, S., Journet, E., and Rajot, J. L.: Mapping the physicochemical properties of mineral dust in western Africa: mineralogical composition, Atmos. Chem. Phys., 14, 10663–10686, https://doi.org/10.5194/acp-14-10663-2014, 2014.

Formenti, P., Piketh, S. J., Namwoonde, A., Klopper, D., Burger, R., Cazaunau, M., Feron, A., Gaimoz, C., Broccardo, S., Walton, N., Desboeufs, K., Siour, G., Hanghome, M., Mafwila, S., Omoregie, E., Junkermann, W., and Maenhaut, W.: Three years of measurements of light-absorbing aerosols over coastal Namibia: seasonality, origin, and transport, Atmos. Chem. Phys., 18, 17003–17016, https://doi.org/10.5194/acp-18-17003-2018, 2018.

Formenti, P., D'Anna, B., Flamant, C., Mallet, M., Piketh, S. J., Schepanski, K., Waquet, F., Auriol, F., Brogniez, G., Burnet, F., Chaboureau, J., Chauvigné, A., Chazette, P., Denjean, C., Desboeufs, K., Doussin, J., Elguindi, N., Feuerstein, S., Gaetani, M., Giorio, C., Klopper, D., Mallet, M. D., Nabat, P., Monod, A., Solmon, F., Namwoonde, A., Chikwililwa, C., Mushi, R., Welton, E. J., and Holben, B.: The Aerosols, Radiation and Clouds in Southern Africa Field Campaign in Namibia: Overview, Illustrative Observations, and Way Forward, B. Am. Meteorol. Soc., 100, 1277–1298, https://doi.org/10.1175/BAMS-D-17-0278.1, 2019.

Formenti, P.: Atmospheric concentrations of total and dissolved elements and water-soluble ions measured over coastal Namibia in 2017, EaSy Data [data set], https://doi.org/10.57932/2ac79cd1-282a-4004-87d5-38f0ebcaf40c, 2023.

Gao, Y., Xu, G., Zhan, J., Zhang, J., Li, W., Lin, Q., Chen, L., and Lin, H.: Spatial and particle size distributions of atmospheric dissolvable iron in aerosols and its input to the Southern Ocean and coastal East Antarctica, J. Geophys. Res., 118, 12634–12648, https://doi.org/10.1002/2013JD020367, 2013.

Gili, S., Vanderstraeten, A., Chaput, A., King, J., Gaiero, D. M., Delmonte, B., Vallelonga, P. F., Di-Biagio, C., Cazaunau, M., Pangui, E., Doussin, J.-F., and Mattielli, N.: South African dust contribution to the high southern latitudes and East Antarctica during interglacial stages, Commun. Earth Environ., 3, 129, https://doi.org/10.1038/s43247-022-00464-z, 2022.

Ginoux, P., Prospero, J. M., Gill, T. E., Hsu, N. C., and Zhao, M.: Global-scale attribution of anthropogenic and natural dust sources and their emission rates based on MODIS Deep Blue aerosols products, Rev. Geophys., 50, RG3005, https://doi.org/10.1029/2012RG000388, 2012.

Giorio, C., Doussin, J. F., D'Anna, B., Mas, S., Filippi, D., Denjean, C., Mallet, M. D., Bourrianne, T., Burnet, F, Cazanaur, M., Chikwililwa, C., Desboeufs, K., Feron, A., Michoud, V., Namwoonde, A., Andreae, M. O., Piketh, S. J., and Formenti, P.: Butene emissions from coastal ecosystems may contribute to new

particle formation, Geophys. Res. Lett., 49, e2022GL098770, https://doi.org/10.1029/2022GL098770, 2022.

Grini, A., Tulet, P., and Gomes, L.: Dusty weather forecasts using the MesoNH mesoscale atmospheric model, J. Geophys. Res., 111, D19205, https://doi.org/10.1029/2005JD007007, 2006.

Guieu, C., Bozec, Y., Blain, S., Ridame, C., Sarthou, G., and Leblond, N.: Impact of high Saharan dust inputs on dissolved iron concentrations in the Mediterranean Sea, Geophys. Res. Lett., 29, 1911, https://doi.org/10.1029/2001GL014454, 2002.

Hamilton, D. S., Perron, M. M. G., Bond, T. C., Bowie, A. R., Buchholz, R. R., Guieu, C., Ito, A., Maenhaut, W., Myriokefalitakis, S., Olgun, N., Rathod, S. D., Schepanski, K., Tagliabue, A., Wagner, R., and Mahowald, N. M.: Earth, wind, fire, and pollution: Aerosol nutrient sources and impacts on ocean biogeochemistry, Annu. Rev. Mar. Sci., 14, 303–330, https://doi.org/10.1146/annurev-marine-031921-013612, 2021.

Heike, K. and Volkel, J.: Soil clay minerals in Namibia and their significance for the terrestrial and marine past global change, African Study Monographs, Suppl. 40, 31–50, https://doi.org/10.14989/96299, 2010.

Heimburger, A., Losno, R., and Triquet, S.: Solubility of iron and other trace elements in rainwater collected on the Kerguelen Islands (South Indian Ocean), Biogeosciences, 10, 6617–6628, https://doi.org/10.5194/bg-10-6617-2013, 2013.

Hooper, H., Mayewski, P., Marx, S., Henson, S., Potocki, M., Sneed, S., Handley, M., Gasso, S., Fischer, M., and Saunders, K. M.: Examining links between dust deposition and phytoplankton response using ice cores, Aeolian Res., 36, 45–60, https://doi.org/10.1016/j.aeolia.2018.11.001, 2019.

Ito, A. and Kok, J. F.: Do dust emissions from sparsely vegetated regions dominate atmospheric iron supply to the Southern Ocean?, J. Geophys. Res., 122, 3987–4002, https://doi.org/10.1002/2016JD025939, 2017.

Ito, A., Ye, Y., Baldo, C., and Shi, Z.: Ocean Fertilization by Pyrogenic Aerosol Iron, NPJ Clim. Atmos. Sci., 4, 30, https://doi.org/10.1038/s41612-021-00185-8, 2021.

Jickells, T., Andersen, K. K., Baker, A., Bergametti, G., Brooks, N., Cao, J., Boyd, P., Duce, R., and Hunter, K.: Global iron connections between desert dust, ocean biogeochemistry, and climate, Science, 308, 67–71, https://doi.org/10.1126/science.1105959, 2005.

Journet, E., Desboeufs, K., Caquineau, S., and Colin, J. L.: Mineralogy as a critical factor of dust iron solublity, Geophys. Res. Lett., 35, L07805, https://doi.org/10.1029/2007GL031589, 2008.

Johansen, A. M. and Key, J. M.: Photoreductive dissolution of ferrihydrite by methanesulfinic acid: Evidence of a direct link between dimethylsulfide and iron-bioavailability, Geophys. Res. Lett., 33, L14818, https://doi.org/10.1029/2006GL026010, 2006.

Kaplan, J. O., Bigelow, N. H., Prentice, I. C., Harrison, S. P., Bartlein, P. J., Christensen, T. R., Cramer, W., Matveyeva, N. V., McGuire, A. D., Murray, D. F., Razzhivin, V. Y., Smith, B., Walker, D. A., Anderson, P. M., Andreev, A. A., Brubaker, L. B., Edwards, M. E., and Lozhkin A. V.: Climate change and Arctic ecosystems: 2. Modeling, paleodata-model comparison and future projections, J. Atmos. Res., 108, 8171, https://doi.org/10.1029/2002JD002559, 2003.

Kangueehi, K. I.: Southern African dust characteristics and potential impacts on the surrounding oceans, PhD thesis, Stellenbosch University, http://hdl.handle.net/10019.1/123923 (last access: 18 January 2024), 2021.

Klopper, D., Formenti, P., Namwoonde, A., Cazaunau, M., Chevaillier, S., Feron, A., Gaimoz, C., Hease, P., Lahmidi, F., Mirande-Bret, C., Triquet, S., Zeng, Z., and Piketh, S. J.: Chemical composition and source apportionment of atmospheric aerosols on the Namibian coast, Atmos. Chem. Phys., 20, 15811–15833, https://doi.org/10.5194/acp-20-15811-2020, 2020.

Kok, J. F., Albani, S., Mahowald, N. M., and Ward, D. S.: An improved dust emission model – Part 2: Evaluation in the Community Earth System Model, with implications for the use of dust source functions, Atmos. Chem. Phys., 14, 13043–13061, https://doi.org/10.5194/acp-14-13043-2014, 2014.

Kok, J. F., Ridley, D. A., Zhou, Q., Miller, R. L., Zhao, C., Heald, C. L., Ward, D. S., Albani, S., and Haustein, K.: Smaller desert dust cooling effect estimated from analysis of dust size and abundance, Nat. Geosci., 10, 274–278, https://doi.org/10.1038/ngeo2912, 2017.

Lafon, S., Sokolik, I. N., Caquineau, S., Rajot, J.-L., and Gaudichet, A.: Characterisation of iron oxides in mineral dust aerosols: implication to light absorption, J. Geophys. Res., 111, D21207, https://doi.org/10.1029/2005JD007016, 2006.

Laurent, B., Marticorena, B., Bergametti, G., Chazette, P., Maignan, F., and Schmechtig C.: Simulation of the mineral dust emission frequencies from desert areas of China and Mongolia using an aerodynamic roughness length map derived from POLDER/ADEOS 1 surface products, J. Geophys. Res., 110, D18S04, https://doi.org/10.1029/2004JD005013, 2005.

Le, S., Josse, J., and Husson, F.: FactoMineR: An R Package for Multivariate Analysis, Journal of Statistical Software [code], 25, 1–18, https://doi.org/10.18637/jss.v025.i01, 2008.

Lide, D. R.: CRC Handbook of Chemistry and Physics 1991–1992, CRC Press, Boca Raton, Florida, ISBN 9781420090840, 1992.

Liu, M., Matsui, H., Hamilton, D. S., Lamb, K. D., Rathod, S. D., Schwarz, J. P., and Mahowald, N. M.: The underappreciated role of anthropogenic sources in atmospheric soluble iron flux to the Southern Ocean, Clim. Atmos. Sci., 5, 28, https://doi.org/10.1038/s41612-022-00250-w, 2022.

Longo, A. F., Feng, Y., Lai, B., Landing, W. M., Shelley, R. U., Nenes, A., Mihalopoulos, N., Violaki, K., and Ingall, E. D.: Influence of Atmospheric Processes on the Solubility and Composition of Iron in Saharan Dust, Environ. Sci. Technol., 50, 6912–6920, https://doi.org/10.1021/acs.est.6b02605, 2016.

Mahowald, N., Luo, C., del Corral, J., and Zender, C. S.: Interannual variablity in atmospheric mineral aerosols from a 22-year model simulation and observational data, J. Geophys. Res.-Atmos., 108, 4352, https://doi.org/10.1029/2002JD002821, 2003.

Marcotte, A. R., Anbar, A. D., Majestic, B. J., and Herckes, P.: Mineral dust and iron solubility: Effects of composition, particle size, and surface area, Atmosphere, 11, 533, https://doi.org/10.3390/atmos11050533, 2020.

Marticorena, B. and Bergametti, G.: Modelling the atmospheric dust cycle: 1. Design of a soil-derived dust emission scheme, J. Geochem. Res., 100, 16415–16430, 1995.

Marticorena, B., Chazette, P., Bergametti, G., Dulac, F., and Legrand, M.: Mapping the aerodynamic roughness length of desert surfaces from the POLDER/ADEOS bi-directional reflectance product, Int. J. Remote Sens., 25, 603–626, 2004.

Myriokefalitakis, S., Tsigaridis, K., Mihalopoulos, N., Sciare, J., Nenes, A., Kawamura, K., Segers, A., and Kanakidou, M.: In-cloud oxalate formation in the global troposphere: a 3-D modeling study, Atmos. Chem. Phys., 11, 5761–5782, https://doi.org/10.5194/acp-11-5761-2011, 2011.

Paris, R. and Desboeufs, K. V.: Effect of atmospheric organic complexation on iron-bearing dust solubility, Atmos. Chem. Phys., 13, 4895–4905, https://doi.org/10.5194/acp-13-4895-2013, 2013.

Paris, R., Desboeufs, K. V., Formenti, P., Nava, S., and Chou, C.: Chemical characterisation of iron in dust and biomass burning aerosols during AMMA-SOP0/DABEX: implication for iron solubility, Atmos. Chem. Phys., 10, 4273–4282, https://doi.org/10.5194/acp-10-4273-2010, 2010.

Paris, R., Desboeufs, K. V., and Journet, E.: Variability of dust iron solubility in atmospheric waters: Investigation of the role of oxalate organic complexation, Atmos. Environ., 45, 6510–6517, https://doi.org/10.1016/j.atmosenv.2011.08.068, 2011.

Perron, M. M. G., Strzelec, M., Gault-Ringold, M., Proemse, B. C., Boyd, P. W., and Bowie, A. R.: Assessment of leaching protocols to determine the solubility of trace metals in aerosols, Talanta, 208, 120377, https://doi.org/10.1016/j.talanta.2019.120377, 2020.

Prospero, J. M., Ginoux, P., Torres, O., Nicholson, S. E., and Gill, T. M.: Environmental characterization of global sources of atmospheric soil dust identified with the Nimbus 7 total ozone mapping spectrometer (TOMS) absorbing aerosol product, Rev. Geophys., 40, 1002, https://doi.org/10.1029/2000RG000095, 2002.

Redemann, J., Wood, R., Zuidema, P., Doherty, S. J., Luna, B., LeBlanc, S. E., Diamond, M. S., Shinozuka, Y., Chang, I. Y., Ueyama, R., Pfister, L., Ryoo, J.-M., Dobracki, A. N., da Silva, A. M., Longo, K. M., Kacenelenbogen, M. S., Flynn, C. J., Pistone, K., Knox, N. M., Piketh, S. J., Haywood, J. M., Formenti, P., Mallet, M., Stier, P., Ackerman, A. S., Bauer, S. E., Fridlind, A. M., Carmichael, G. R., Saide, P. E., Ferrada, G. A., Howell, S. G., Freitag, S., Cairns, B., Holben, B. N., Knobelspiesse, K. D., Tanelli, S., L'Ecuyer, T. S., Dzambo, A. M., Sy, O. O., McFarquhar, G. M., Poellot, M. R., Gupta, S., O'Brien, J. R., Nenes, A., Kacarab, M., Wong, J. P. S., Small-Griswold, J. D., Thornhill, K. L., Noone, D., Podolske, J. R., Schmidt, K. S., Pilewskie, P., Chen, H., Cochrane, S. P., Sedlacek, A. J., Lang, T. J., Stith, E., Segal-Rozenhaimer, M., Ferrare, R. A., Burton, S. P., Hostetler, C. A., Diner, D. J., Seidel, F. C., Platnick, S. E., Myers, J. S., Meyer, K. G., Spangenberg, D. A., Maring, H., and Gao, L.: An overview of the ORACLES (ObseRvations of Aerosols above CLouds and their intEractionS) project: aerosol–cloud–radiation interactions in the southeast Atlantic basin, Atmos. Chem. Phys., 21, 1507–1563, https://doi.org/10.5194/acp-21-1507-2021, 2021.

Reichholf, J. H.: Is Saharan Dust a Major Source of Nutrients for the Amazonian Rain Forest?, Stud. Neotrop. Fauna E., 21, 251–255, https://doi.org/10.1080/01650528609360710, 1986.

Rodríguez, S., Prospero, J. M., Lopez-Darias, J., Garcia-Alvarez, M. I., Zuidema, P., Nava, S., Lucarelli, F., Gaston, C. J., Galindo, L., and Sosa, E.: Tracking the changes of iron solubility and air pollutants traces as African dust transits the Atlantic in the Saharan dust outbreaks, Atmos. Environ., 246, 118092, https://doi.org/10.1016/j.atmosenv.2020.118092, 2021.

Rodríguez, S., Riera, R., Fonteneau, A., Alonso-Pérez, S., and López-Darias, J.: African desert dust influences migrations and fisheries of the Atlantic skipjack-tuna, Atmos. Environ., 312, 120022, https://doi.org/10.1016/j.atmosenv.2023.120022, 2023.

Rudnick, R. L. and Gao, S.: Composition of the Continental Crust, in: Treatise on Geochemistry, edited by: Holland, H. D. and Turekian, K. K., Elsevier, Amsterdam, Vol. 3, 64 pp., ISBN 0-08-043751-6, 2004.

Shelley, R. U., Morton, P. L., and Landing, W. M.: Elemental ratios and enrichment factors in aerosols from the US-GEOTRACES North Atlantic transects, Deep-Sea Res. II, 116, 262–272, https://doi.org/10.1016/j.dsr2.2014.12.005, 2015.

Shelley, R. U., Landing, W. M., Ussher, S. J., Planquette, H., and Sarthou, G.: Regional trends in the fractional solubility of Fe and other metals from North Atlantic aerosols (GEOTRACES cruises GA01 and GA03) following a two-stage leach, Biogeosciences, 15, 2271–2288, https://doi.org/10.5194/bg-15-2271-2018, 2018.

Sholkovitz, E. R., Sedwick, P. N., and Church, T. M.: Influence of anthropogenic combustion emissions on the deposition of soluble aerosol iron to the ocean: empirical estimates for island sites in the North Atlantic, Geochim. Cosmochim. Ac., 73, 3981–4003, https://doi.org/10.1016/j.gca.2009.04.029, 2009.

Siefert, R. L., Pehkonen, S. O., Erel, Y., and Hoffman, M. R.: Iron photochemistry of aqueous suspensions of ambient aerosol with added organic acids, Geochim. Cosmochim. Ac,, 58, 3271–3279, 1994.

Spirig, R., Vogt, R., Larsen, J. A., Feigenwinter, C., Wicki, A., Franceschi, J., Parlow, E., Adler, B., Kalthoff, N., Cermak, J., Andersen, H., Fuchs, J., Bott, A., Hacker, M., Wagner, N., Maggs-Kölling, G., Wassenaar, T., and Seely, M.: Probing the fog life-cycles in the Namib desert, B. Am. Meteorol. Soc., 100, 2491–2508, https://doi.org/10.1175/bams-d-18-0142.1, 2019.

Swan, H. B. and Ivey, J. P.: Elevated particulate methanesulfonate, oxalate and iron over Sydney Harbour in the austral summer of 2019–20 during unprecedent bushfire activity, Atmos. Environ., 226, 118739, https://doi.org/10.1016/j.atmosenv.2021.118739, 2021.

Swap, R., Garstang, M., Macko, S. A., Tyson, P. D., Maenhaut, W., Artaxo, P., Kållberg, P., and Talbot, R.: The long-range transport of southern African aerosols to the tropical South Atlantic, J. Geophys. Res., 101, 23777–23791, https://doi.org/10.1029/95jd01049, 1996.

Takahashi, Y., Higashi, M., Furukawa, T., and Mitsunobu, S.: Change of iron species and iron solubility in Asian dust during the long-range transport from western China to Japan, Atmos. Chem. Phys., 11, 11237–11252, https://doi.org/10.5194/acp-11-11237-2011, 2011.

Tao, Y. and Murphy, J. G.: The mechanisms responsible for the interactions among oxalate, pH, and Fe dissolution in $PM_{2.5}$, Earth Space Chem., 3, 2259–2265, https://doi.org/10.1021/acsearthspacechem.9b00172, 2019.

Taylor, S. R. and S. M. McLennan: The geochemical evolution of the continental crust, Rev. Geophys., 33, 241–265, https://doi.org/10.1029/95RG00262, 1995

Tegen, I. and Schepanski, K.: The Global distribution of Mineral Dust, IOP C. Ser. Earth Env., 7, 012001, https://doi.org/10.1088/1755-1307/7/1/012001, 2009.

Tyson, P. D. and Preston-Whyte, R. A.: The Weather and Climate of Southern Africa, 2nd edn., Oxford University Press Southern Africa, Cape Town, ISBN 0-19-571806-2, 2014.

Ventura, A., Simões, E. F. C., Almeida, A. S., Martins, R., Duarte, A. C., Loureiro, S., and Duarte, R. M. B. O.: Deposition of aerosols onto upper ocean and their impacts on marine biota, Atmosphere, 12, 684, https://doi.org/10.3390/atmos12060684, 2021.

Vickery, K. J. and Eckardt, F. D.: Dust emission controls on the lower Kuiseb River valley, Central Namib, Aeolian Res., 10, 125–133, https://doi.org/10.1016/j.aeolia.2013.02.006, 2013.

von Holdt, J. R., Eckardt, F. D., and Wiggs, G. F. S.: Landsat identifies aeolian dust emission dynamics at the landform scale, Remote Sens. Environ., 198, 229–243, https://doi.org/10.1016/j.rse.2017.06.010, 2017.

Wozniak, A. S., Shelley, R. U., Sleighter, R. L., Abdulla, H. A. N., Morton, P. L., Landing, W. M., and Hatcher, P. G.: Relationships among aerosol water soluble organic matter, iron and aluminium in European, North African, and Marine air masses from the 2010 US GEOTRACES cruise, Mar. Chem., 154, 24–33, https://doi.org/10.1016/j.marchem.2013.04.011, 2013.

Wozniak, A. S., Shelley, R. U., McElhenie, S. D., Landing, W. M., Hatcher, P. G.: Aerosol water soluble organic matter characteristics over the North Atlantic Ocean: Implications for iron-binding ligands and iron solubility, Mar. Chem. 173, 162–172, https://doi.org/10.1016/j.marchem.2014.11.002, 2015.

Zhuang, G., Yi, Z., Duce, R. A., and Brown, P. R.: Link between iron and sulphur cycles suggested by detection of Fe (II) in remote marine aerosols, Nature, 355, 537–539, https://doi.org/10.1038/355537a0, 1992.

Supplement of Atmos. Chem. Phys., 24, 1525–1541, 2024
https://doi.org/10.5194/acp-24-1525-2024-supplement

Atmospheric Chemistry and Physics
Open Access
EGU

Supplement of

Fractional solubility of iron in mineral dust aerosols over coastal Namibia: a link to marine biogenic emissions?

Karine Desboeufs et al.

Correspondence to: Paola Formenti (paola.formenti@lisa.ipsl.fr)

Fig S1. *Composite of ancillary information on dust episodes from modelling and remote sensing. Left: maps of episode-averaged dust emission flux at a 0.1° x 0.1° grid calculated as in described by Feuerstein and Schepanski (2019). Values are expressed in kg m^{-2} day^{-1}; Middle: maps of dust optical depth (shading) and 10-m wind (vector) overlaid by pathway of 21-hour air mass back trajectories ending in the first 100 m (red line) and between 200 and 300 m (blue line) above HBAO as calculated by the Meso-NH model (version 5.3). Dots are plotted every hour and shadings around these lines are the interquartile ranges for latitudes. Right: fractional average fog and low cloud coverage during the period of the dust episodes (see Table 1).*

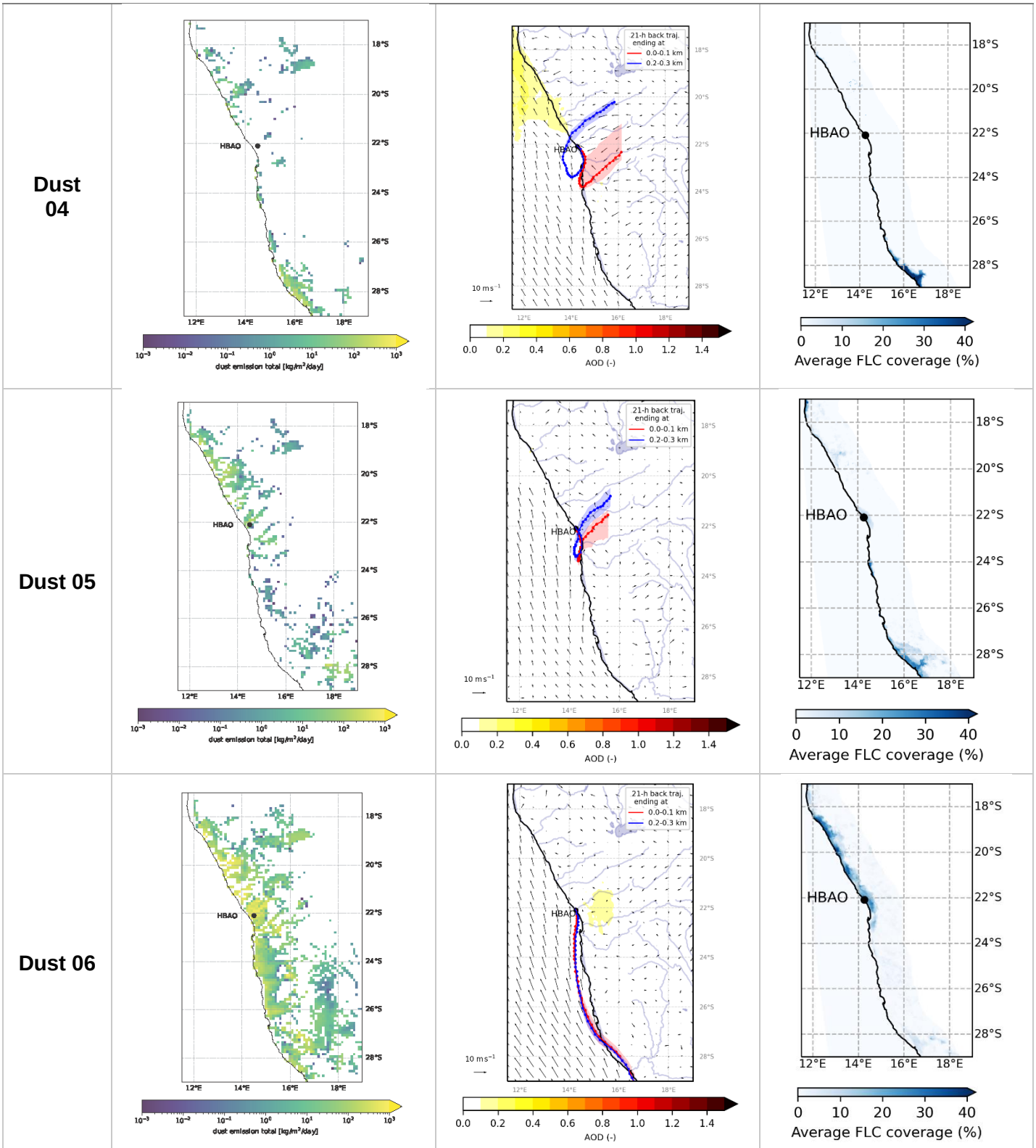

Dust 07	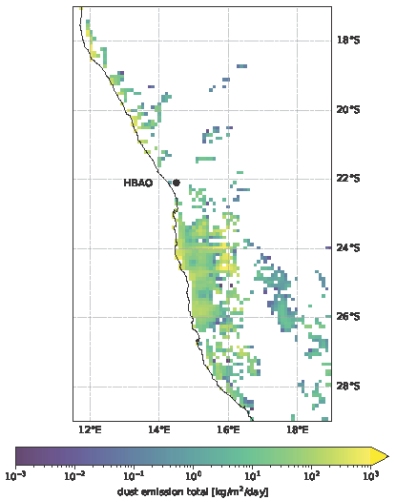	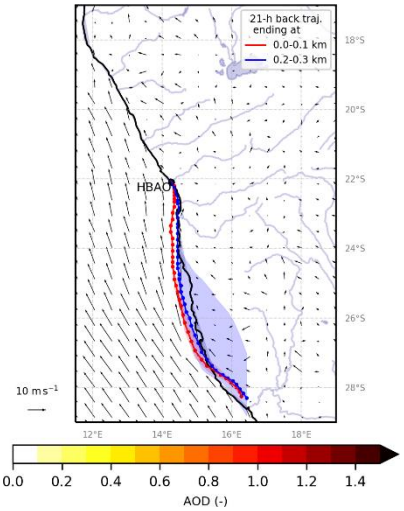	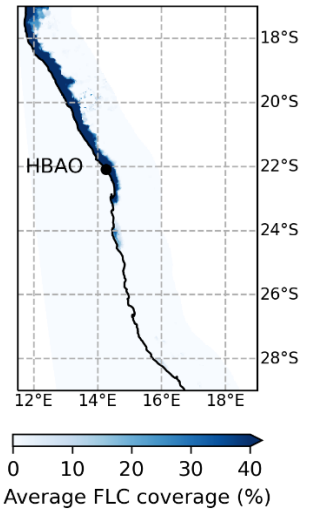
Dust 08	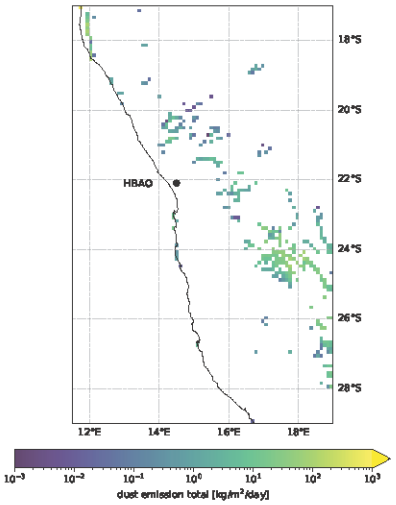	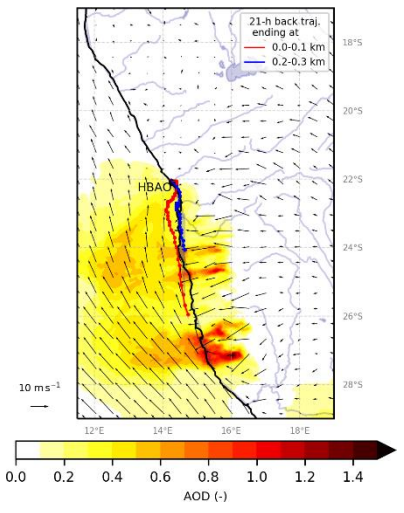	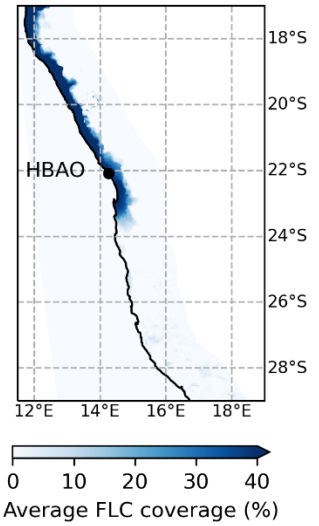
Dust 09	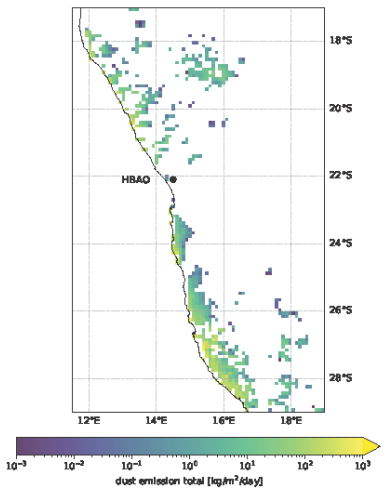	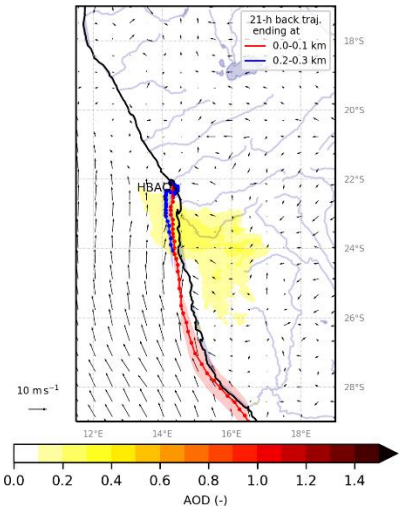	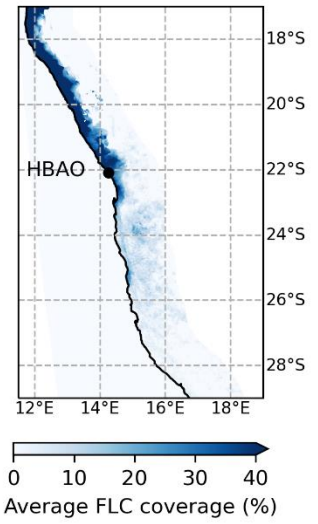

Dust 10	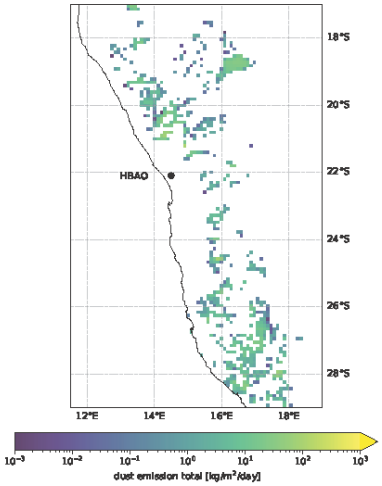	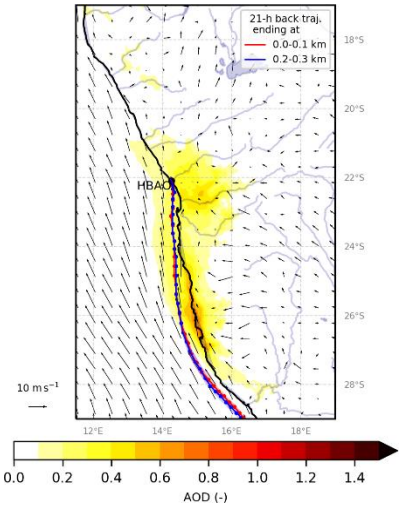	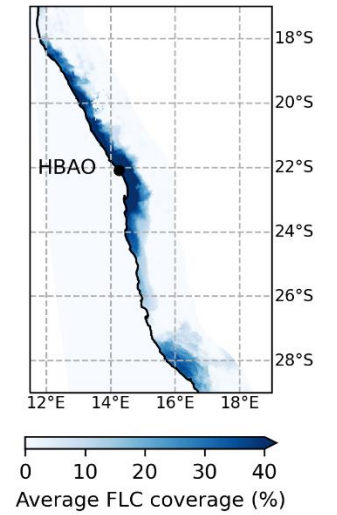
Dust 11	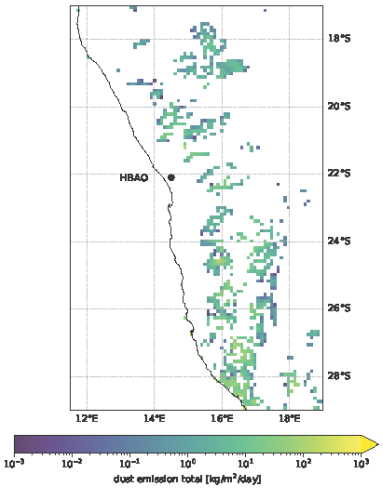	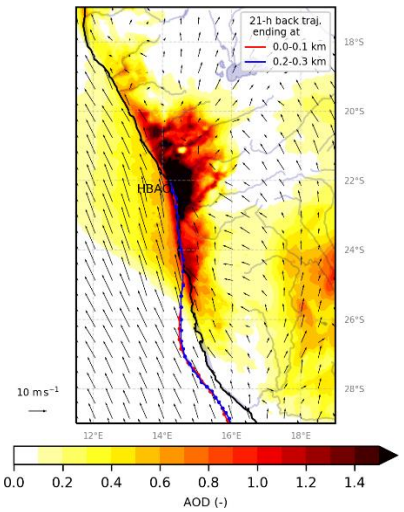	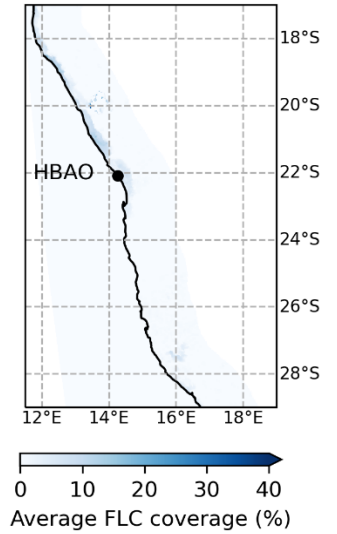
Dust 12	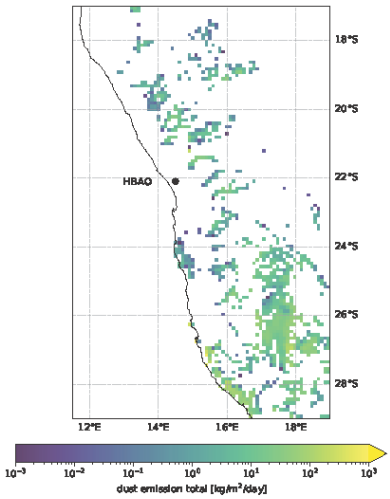	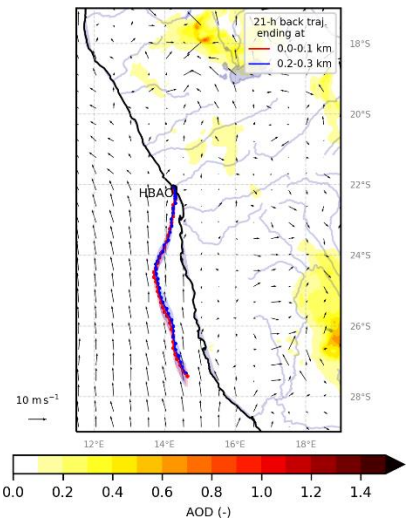	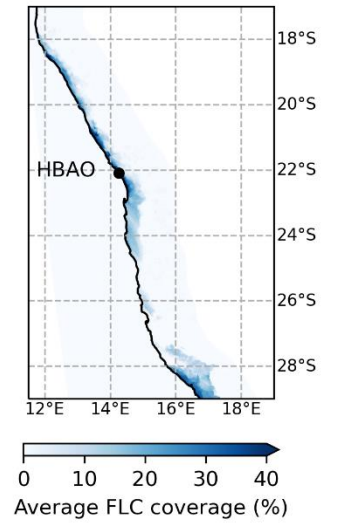

Dust 13	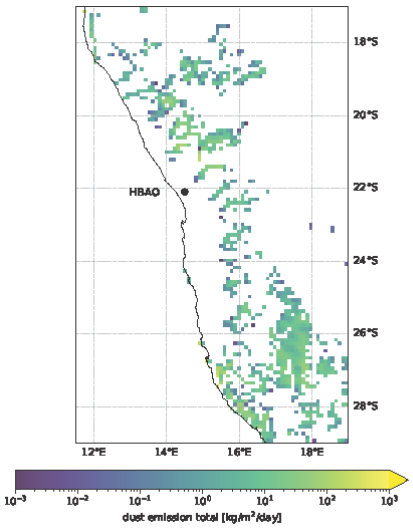	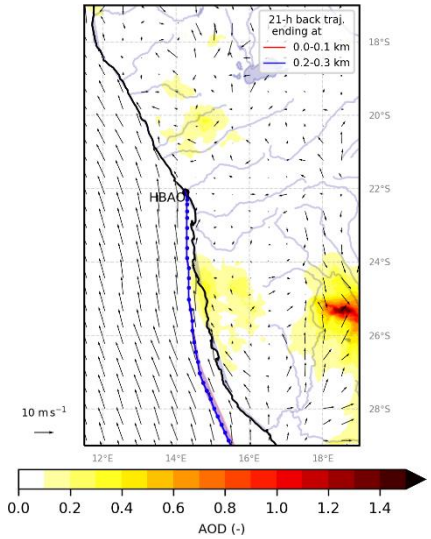	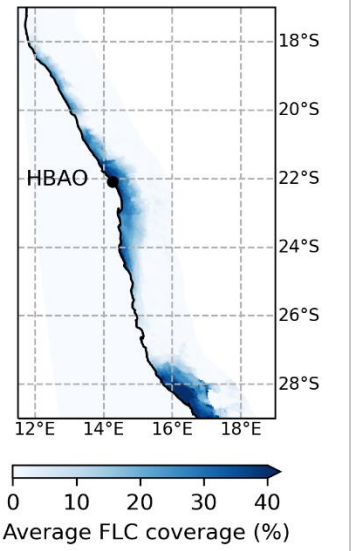

18
19

20

Fig.S2. *Temporal evolution of meteorological parameters during the different periods of sampling. IBox indicates the interquartile range, i.e. the 25th and the 75th percentile, and the line within the box marks the median. Whiskers indicate the quartiles ±1.5 times the interquartile range. Points above and below the whiskers indicate outliers outside the 10th and 90th percentile.*

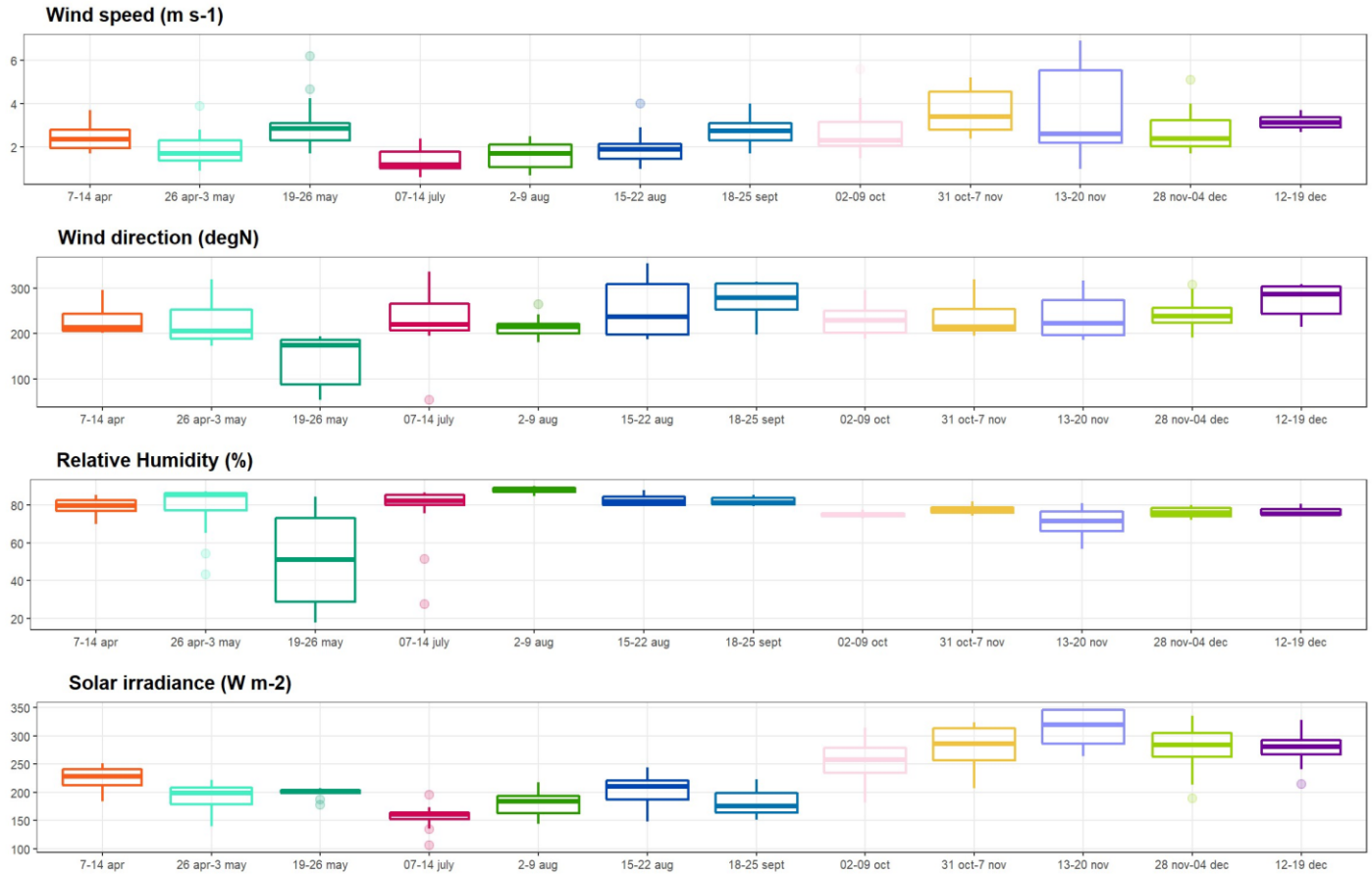

Fig S3. *Time series of the Si/Al (top panel) and of the Fe/nss-Ca (lower panel) ratios measured during April and December 2017 at HBAO. Background and dust samples are represented in blue and grey, respectively. Boxes indicate the interquartile range, i.e. the 25th and the 75th percentile, and the line within the box marks the median. Whiskers indicate the quartiles ±1.5 times the interquartile range. Points above and below the whiskers indicate outliers outside the 10th and 90th percentile.*

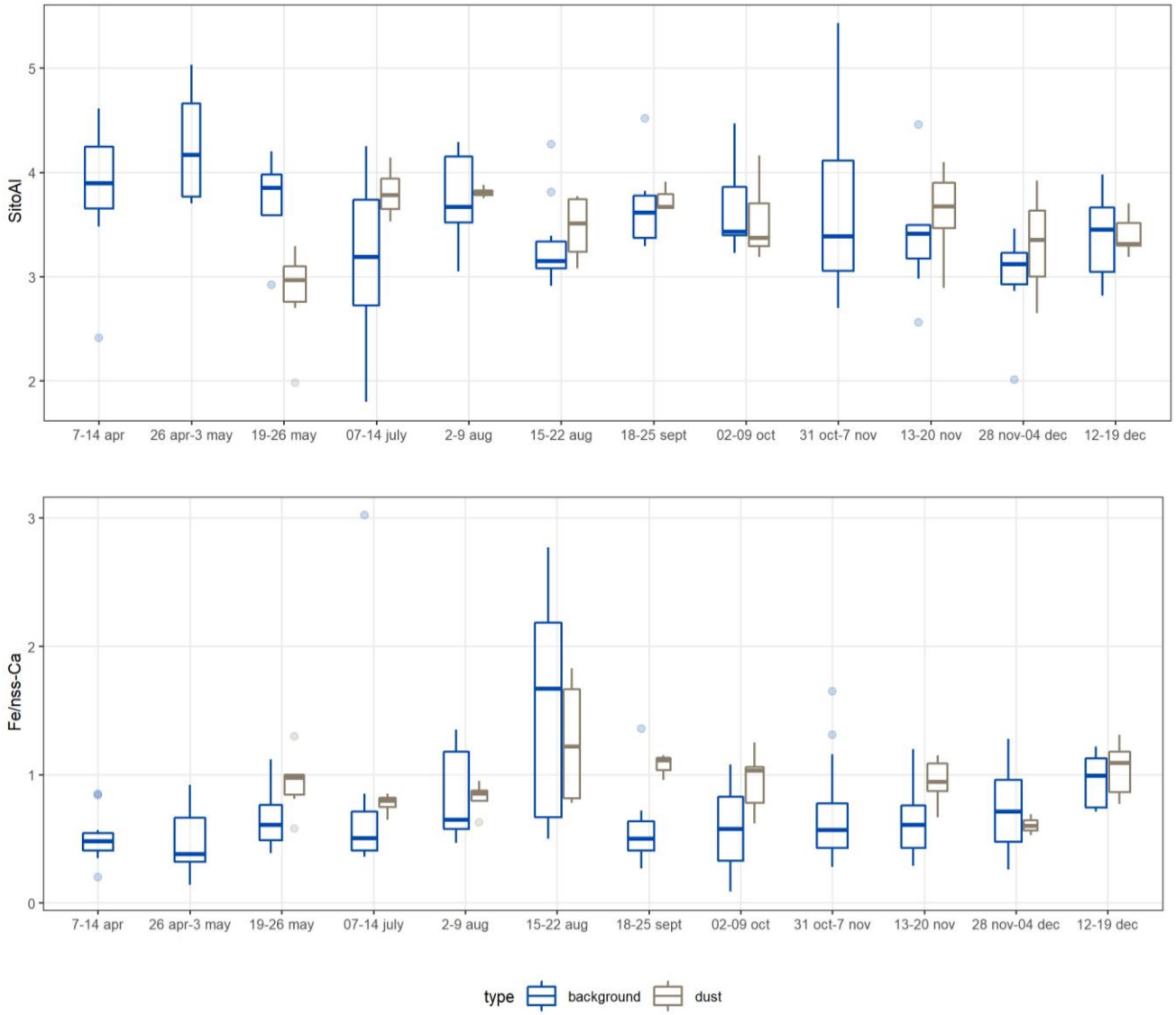

Fig. S4: *Dependence of %SFe and secondary compounds concentrations for background (grey dots) and dust (orange dots) samples:*

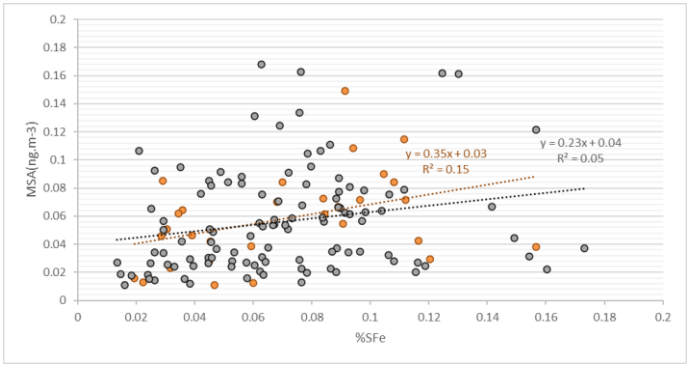

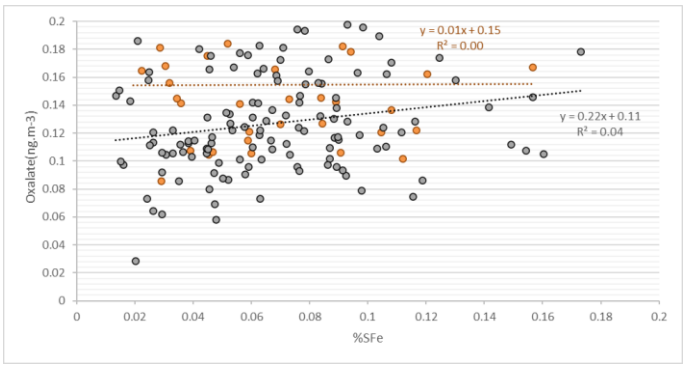

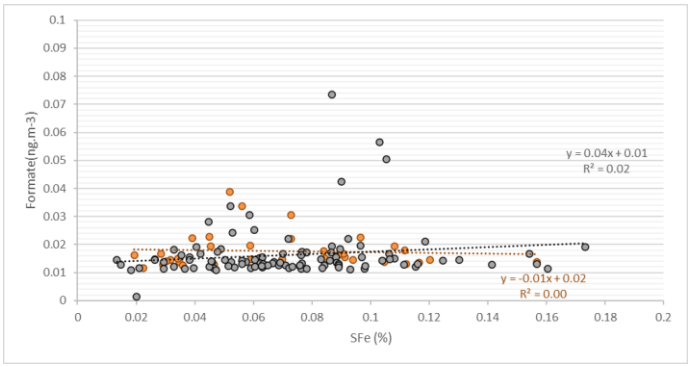

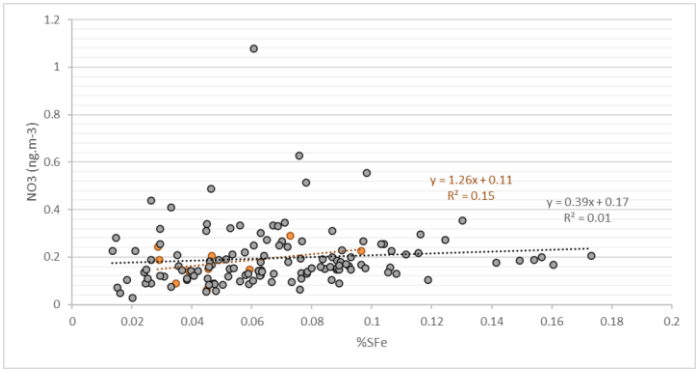

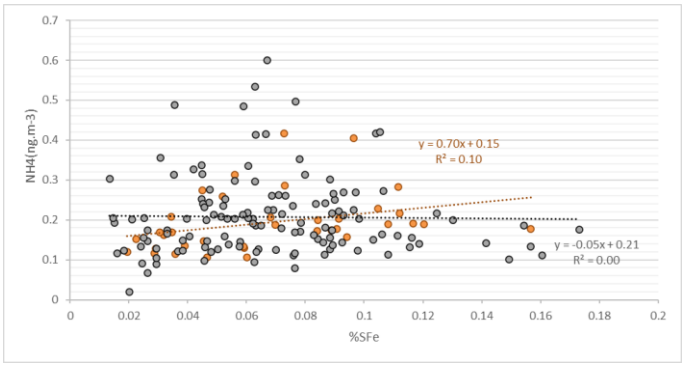

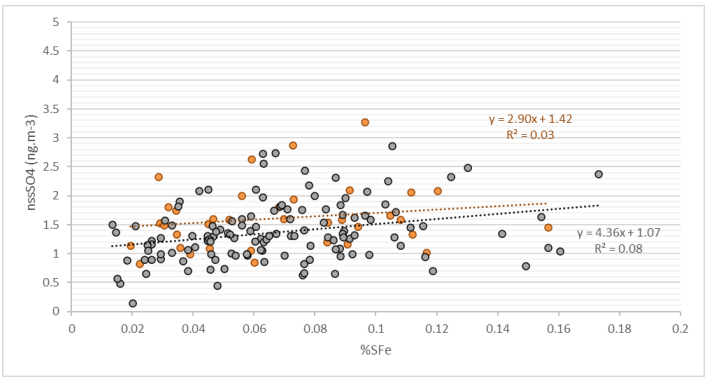

Fig S5. *Dependence of MSA (top) and iron fractional solubility (bottom) on wind speed and solar irradiance during the dust events (orange dots) and background periods (blue doots).*

.